AD-A087 278 IRT CORP SAN DIEGO CA F/G 20/7
INVESTIGATION OF ELECTRON ATTACHMENT IN POLYATOMIC MOLECULES.(U)
MAY 80 J T DOWELL F49620-77-C-0071
UNCLASSIFIED IRT-8164-004 AFOSR-TR-80-0549 NL

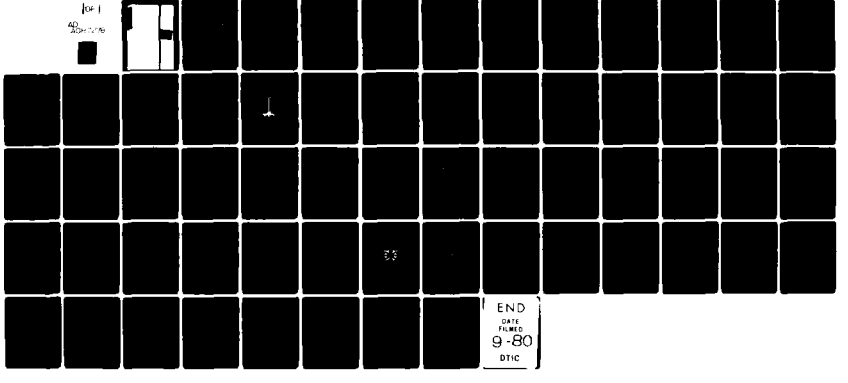

END
DATE FILMED
9-80
DTIC

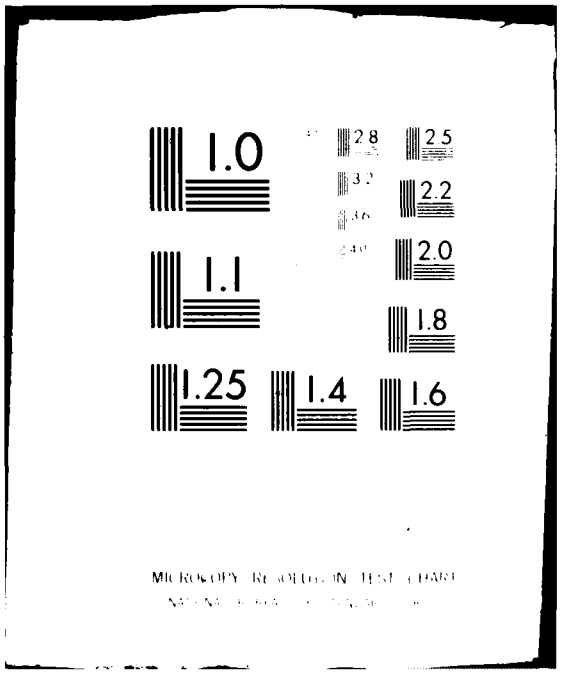
1.0
2.8
2.5
3.2
2.2
3.6
4.0
2.0
1.1
1.8
1.25
1.4
1.6
MICROCOPY RESOLUTION TEST CHART

AFOSR-TR- 80-0549

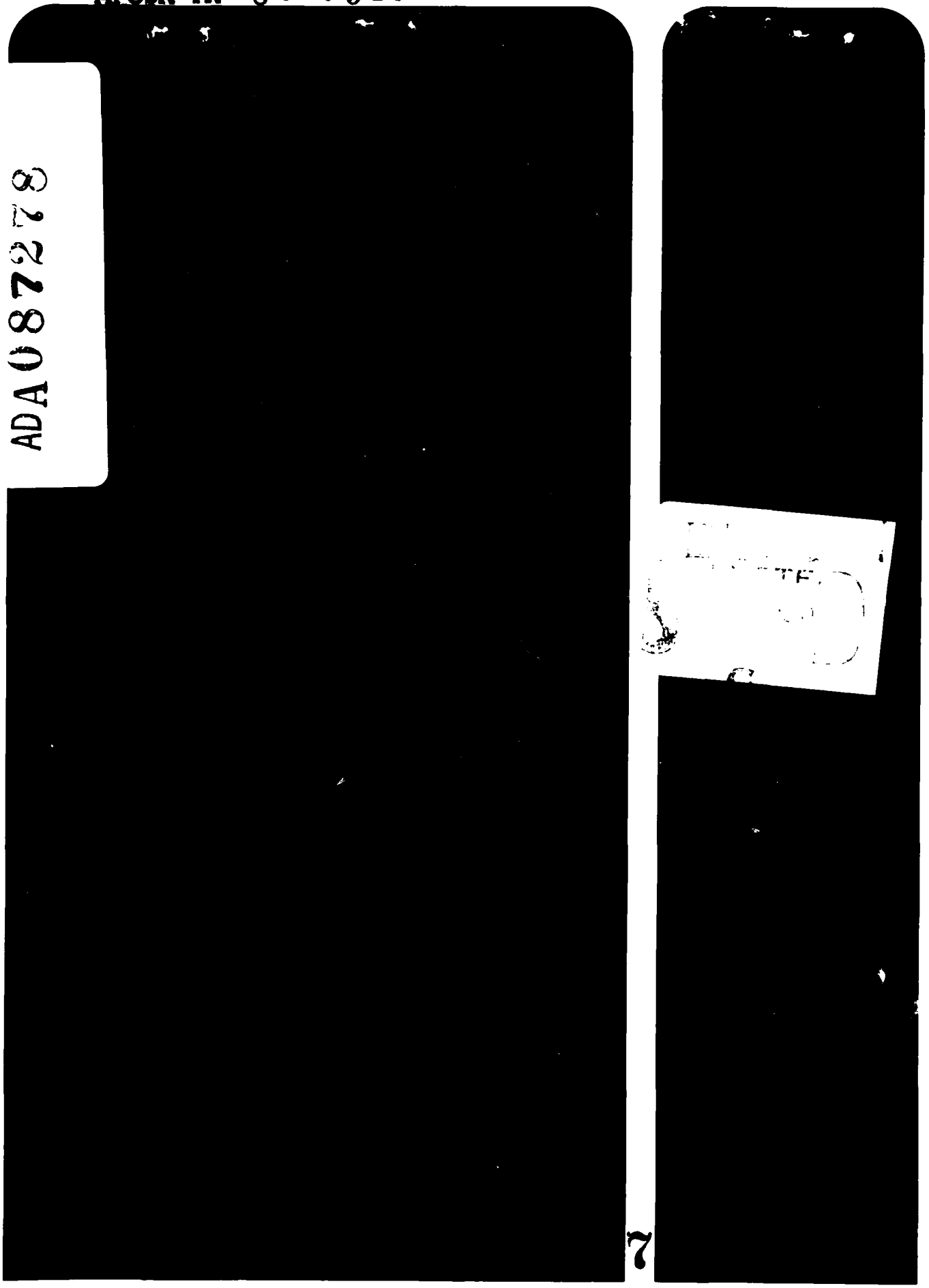

ADA087278

7

IRT 8164-004

INVESTIGATION OF ELECTRON ATTACHMENT IN POLYATOMIC MOLECULES

FINAL REPORT
1 April 1977 - 31 March 1980

Contract Number: F49620-77-C-0071
Principal Investigator: Dr. J. T. Dowell

Sponsored by
AIR FORCE OFFICE OF SCIENTIFIC RESEARCH

May 30, 1980

AIR FORCE OFFICE OF SCIENTIFIC RESEARCH (AFSC)
NOTICE OF TRANSMITTAL TO DDC
This technical report has been reviewed and is
approved for public release IAW AFR 190-12 (7b).
Distribution is unlimited.
A. D. BLOSE
Technical Information Officer

DTIC
ELECTE
JUL 3 0 1980
S D
C

IRT Corporation

Instrumentation
Research
Technology

7650 Convoy Court • P.O. Box 80817
San Diego, California 92138

714 / 565-7171
Telex 69-5412

UNCLASSIFIED

SECURITY CLASSIFICATION OF THIS PAGE (When Data Entered)

REPORT DOCUMENTATION PAGE	READ INSTRUCTIONS BEFORE COMPLETING FORM
1. REPORT NUMBER: AFOSR-TR-80-0549	2. GOVT ACCESSION NO.: AD-A087278	3. RECIPIENT'S CATALOG NUMBER
4. TITLE (and Subtitle): INVESTIGATION OF ELECTRON ATTACHMENT IN POLYATOMIC MOLECULES.	5. TYPE OF REPORT & PERIOD COVERED: Final Report. 1 Apr 77 — 31 Mar 80
	6. PERFORMING ORG. REPORT NUMBER: IRT 8164-004
7. AUTHOR(s): Jerry T. Dowell	8. CONTRACT OR GRANT NUMBER(s): F49620-77-C-0071
9. PERFORMING ORGANIZATION NAME AND ADDRESS: IRT Corporation, P.O. Box 80817, San Diego, CA 92138	10. PROGRAM ELEMENT, PROJECT, TASK AREA & WORK UNIT NUMBERS: 2303/B1, 61102F, B1
11. CONTROLLING OFFICE NAME AND ADDRESS: Air Force Office of Scientific Research, Bldg. 410, Bolling AFB, DC 20332	12. REPORT DATE: May 1980; 13. NUMBER OF PAGES: 60
14. MONITORING AGENCY NAME & ADDRESS (if different from Controlling Office)	15. SECURITY CLASS (of this report): UNCLASSIFIED; 15a. DECLASSIFICATION/DOWNGRADING SCHEDULE

16. DISTRIBUTION STATEMENT (of this Report)

Approved for public release; distribution unlimited.

17. DISTRIBUTION STATEMENT (of the abstract entered in Block 20, if different from Report)

18. SUPPLEMENTARY NOTES

19. KEY WORDS (Continue on reverse side if necessary and identify by block number)

Molecular Beams
Electron Beams
Electron Attachment
Sulfur Hexafluoride
Molybdenum Hexafluoride
Tungsten Oxide

20. ABSTRACT (Continue on reverse side if necessary and identify by block number)

Electron attachment to polyatomic molecules was studied using molecular beams of variable temperature crossed with an electron beam of high energy resolution. Species investigated include sulfur hexafluoride, molybdenum hexafluoride, and tungsten oxide polymers. New results were obtained in sulfur hexafluoride demonstrating the importance of internal energy for the dissociative attachment process. A strong temperature dependence was observed for direct attachment in molybdenum hexafluoride. Tungsten oxide vapor exhibits both monomer and dimer negative ion formation near zero energy,

DD FORM 1 JAN 73 1473 EDITION OF 1 NOV 65 IS OBSOLETE

UNCLASSIFIED

SECURITY CLASSIFICATION OF THIS PAGE (When Data Entered)

409388

apparently from dissociative attachment to the trimer.

CONTENTS

Accession For
NTIS GRA&I
DDC TAB
Unannounced
Justification
By
Distribution/
Availability Codes
Dist | Avail and/or special
A

1. INTRODUCTION

The following report is an account of research performed under Contract F49620-77-C-0071 by IRT Corporation during the period 1 April 1977 through 31 March 1980. The Principal Investigator was Dr. Jerry T. Dowell.

The research program was concerned with the investigation of two-body electron attachment processes in molecules. Emphasis in the program was on the study of reactions that appear to have high rates in plasmas and that involve species with high electron affinities. Such reactions were of interest for two reasons: advancement of the theoretical understanding of resonant electron-molecule scattering for other than diatomic molecules, and possible application to plasma engineering (e.g., wake modification).

Two-body attachment reactions are of the following general types:

$$(1)\quad e^- + AB \rightarrow A + B^- \quad \text{(dissociative attachment)} ,$$

or

$$(2)\quad e^- + AB \rightarrow (AB)^- \quad \text{(direct attachment)} ,$$

where A and B may be atoms or molecules, where the ion $(AB)^-$ formed in this manner is at least initially metastable, and where any of the products A, B^-, or $(AB)^-$ may be excited. Dissociative attachment is considered to be a resonant process, viz. the reaction proceeds through a state of the temporary negative ion $(AB)^-$. (In direct attachment, the temporary negative ion is long-lived.) States of the temporary negative ion usually also strongly influence other channels of the electron-molecule scattering, often producing sharp resonances in the elastic and inelastic cross sections (Ref. 1).

Ideally, studies of two-body electron attachment should include measurement of the following:

(1) Variation of attachment cross sections with electron energy, and with gas temperature.

(2) Product negative ion kinetic energies as functions of incident electron energy.

(3) Energies and characteristics of resonances in total scattering.

(4) Attachment rates as functions of temperature.

If the attachment cross sections are measured with sufficiently good electron energy resolution and the measurements extend down to the lowest electron energy at which attachment occurs, then rates may be calculated from the cross section data and experiments to determine them are unnecessary. The cross section for attachment at a particular electron energy may depend very strongly on the state of excitation of the target molecules. The temperature dependence of the attachment rate in a gas may thus not be easily deduced from rate measurements over a limited temperature range, or from attachment cross section measurements in the gas at a fixed temperature. Information on the energetics (e.g., bond energies and electron affinities) of the molecules studied is obtained from the kinetic energy measurements, and investigation of the scattering resonances yields insight into compound states.

The primary technique presently employed in the program is that of crossed molecular and electron beams. A molecular beam of the species of interest is crossed with a monoenergetic electron beam of variable energy, and negative ions formed by two-body attachment in the intersection region are extracted, mass analyzed, and detected. The gas temperature dependence of the cross sections is obtained by variation of the molecular beam source temperature.

A new method, incorporating a quadrupole electron trap, was originally proposed for direct measurements of attachment rates. Briefly, a molecular beam of the species of interest is passed through a cloud of electrons contained in the trap. The attachment rate of electrons to beam molecules is obtained by measurement of the depletion rate of the electrons together with determination of the molecular density in the beam. Some equipment for developing this method was accumulated during the first year of the program (at no cost to the contract), but it was decided that concentration on use of the beam method would be the best course to pursue. For future reference, a description of the electron trap method is included in this report as Appendix A.

Electron attachment to the following species was studied in the program: H_2WO_4, WO_3 vapor, SF_6, MoF_6, and WF_6. The apparatus developed for the project is described in Section 2 and the exploratory experiments are discussed in Section 3. In Section 4, evidence is presented of a discrimination effect that

affects measurements at very low electron energies in a common type of electron geometry. Details of attachment measurements made after curing that discrimination are given in Section 5, which contains the significant results obtained in the program. Some of the studies of MoF_6 and WF_6 are presented in Appendix B, which is a condensed version of a report issued earlier in the program.

2. APPARATUS CONSTRUCTION AND DEVELOPMENT

2.1 MOLECULAR BEAM SYSTEM

Attachment measurements were to be performed in the program by crossing an electron beam with a molecular beam and detecting product negative ions. Consequently, the first part of the experimental apparatus to be developed was the molecular beam source and vacuum system. A prime consideration for the design of the molecular beam apparatus was flexibility in the method of production of the beam and in the types of electron beam and detection techniques that could be used. Thus, the molecular beam source had to be capable of using permanent gases as well as solids over a wide temperature range. The main experimental chamber had to be of sufficient size to accommodate mass spectrometers, consistent with good vacuum.

The IRT Beam Laboratory possesses several molecular beam systems as well as numerous parts of systems. A beam apparatus was assembled from these parts to suit the requirements of the present program. It consisted of three cylindrical, separately pumped chambers - source chamber, buffer chamber, and main chamber. Dimensions of these chambers are given in Table 1. Care was taken to ensure that the main chamber vacuum would be better than 10^{-7} torr, since it was felt that the electron monochromator would not function properly with poor vacuum and that the detection sensitivity for ions would not be high enough. Throughout the program, the main chamber vacuum has been 5×10^{-8} torr or better under operating conditions.

Table 1

Molecular Beam Apparatus Chamber Dimensions

Chamber	OD (cm)	Length (cm)
Source	22.9	38.1
Buffer	33.0	10.8
Main	61.0	66.0

The beam source assembly was mounted on a large vacuum flange so that the source could be rapidly removed from the apparatus for service or modification. In the source assembly, the source oven was mounted from two massive metal supports that are electrically isolated, so that the oven could be directly heated by connecting a low-voltage, high-current transformer to the supports. For most of the experimental work, the ovens were tubular, 0.48 cm dia x 4.3 cm long, with 0.05 cm beam orifice. Gases could be introduced into the oven through stainless steel lines attached to the oven supports, and in addition, the oven was easily detachable for loading with solid material. The entire source assembly could be remotely positioned from outside the vacuum system for rapid beam alignment.

2.2 IONIZER-MASS SPECTROMETER

In the preliminary investigations on tungsten compounds, a means for determination of molecular beam compositions was required. For this purpose, a beam analysis and detection system, consisting of an electron beam ionizer and 180° magnetic mass spectrometer, an electron multiplier, and a solid state preamp, was installed in the main chamber. The basic mechanical design of the ionizer-mass spectrometer is shown in Fig. 1. The electromagnet coils for the mass spectrometer are enclosed in a vacuum-tight, gold-plated can. The pole faces are also gold-plated. The electrodes in the ionizer are constructed of gold-plated soft iron and are located and spaced by 0.075 cm dia sapphire rods in V-grooves. Thus, since the ionizer assembly is attached directly to the pole faces, the magnetic field between the poles is continued in the ionizer, serving to collimate the electron beam. The ionizer exhibits good ionization and ion extraction efficiency and the electron beam is well-behaved for electron accelerating potentials greater than 10 V.

A box-dynode electron multiplier is used for ion current measurement in an AC synchronous detection scheme, wherein the molecular beam is chopped at 100 Hz with a toothed wheel in the buffer chamber before passing into the main chamber and through the ionizer. Ions formed in the ionizer are extracted, mass analyzed, and detected synchronously with the chopper reference signal.

A drawing of the installation of the ionizer-mass spectrometer in a molecular beam apparatus is shown in Fig. 2.

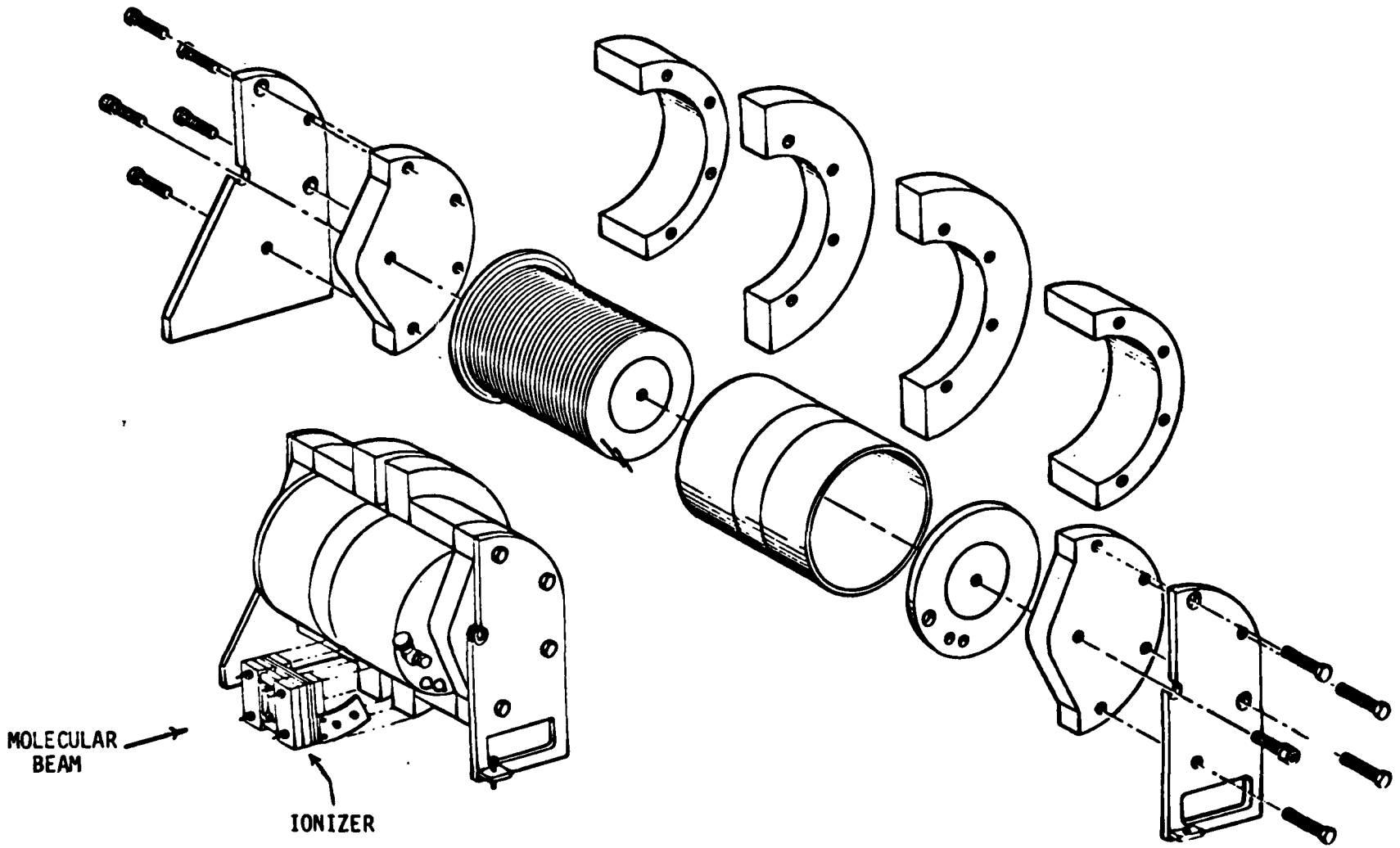

Figure 1. Basic design of ionizer-mass spectrometer system

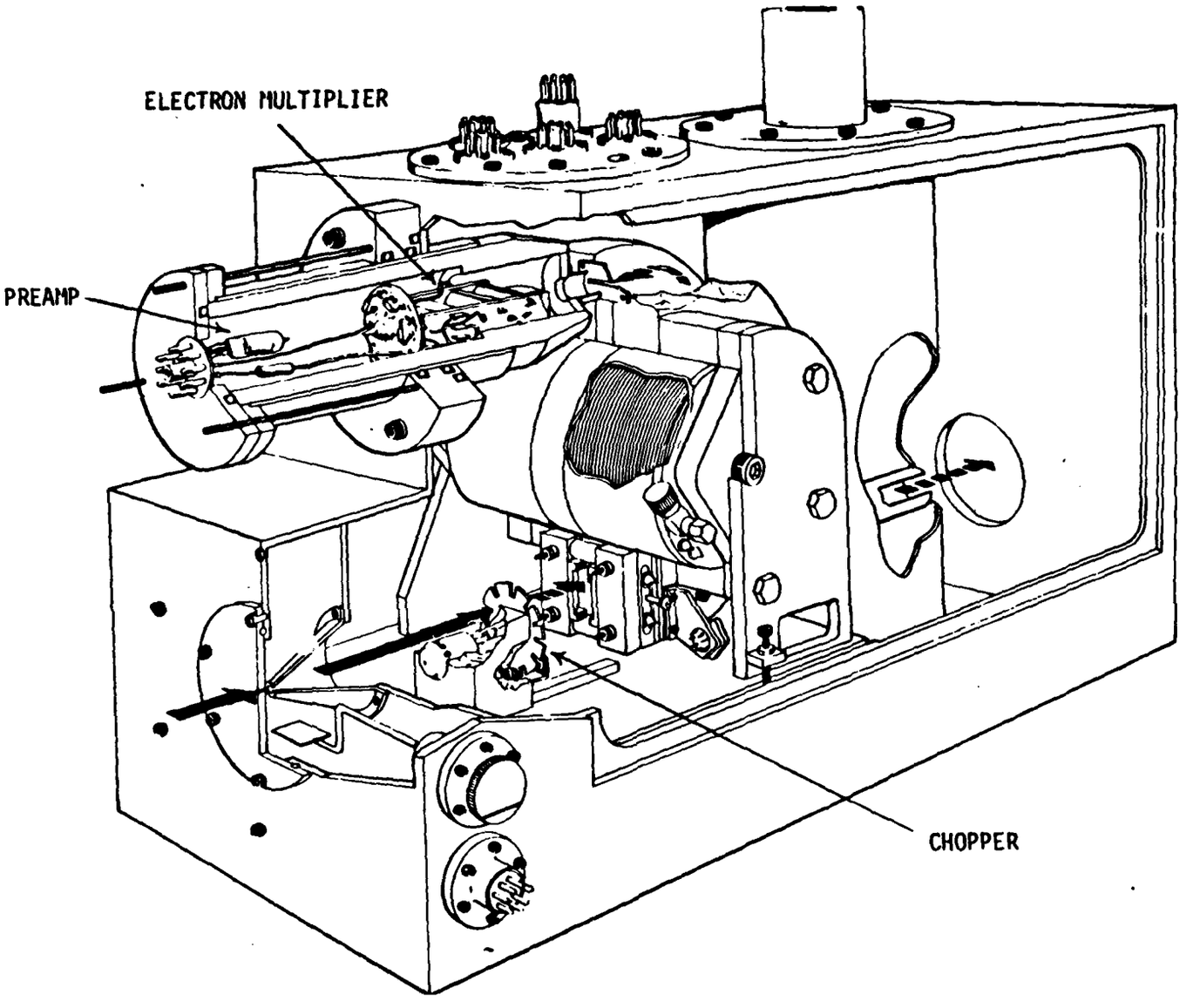

Figure 2. Cut-away view of an ionizer-mass spectrometer system installed in a molecular beam apparatus

2.3 ELECTRON MONOCHROMATOR SYSTEM

Attachment measurements require an electron beam with very small energy spread and with well-behaved operation down to nearly zero electron energy. The most suitable electron gun for this program appeared to be the trochoidal monochromator (Ref. 2). A simplified schematic diagram of such an electron beam system is shown in Fig. 3. Electrons emitted from a thoriated iridium filament are collimated into a beam by an axial magnetic field B (usually 30-100 gauss) and holes in a series of plates. The beam enters a monochromator region M that consists of a pair of parallel plates producing an electric field perpendicular to the magnetic field. Due to the $\vec{E}x\vec{B}$ drift (which is, in general, a trochoidal motion), the electrons are deflected in a direction perpendicular to both the electric and magnetic fields and are dispersed according to their initial velocities. Some of these deflected electrons with a narrow range of velocities pass through a hole (offset from the original axis) as they exit the crossed field region, are accelerated into the collision chamber along the new axis parallel to $\vec{B}$, and are eventually collected after leaving the collision chamber. In the figure, the molecular beam passes perpendicular to the page through the dashed circle in the collision chamber. Further details on operation of the trochoidal monochromator can be found in Ref. 2.

A drawing of the essential features of the electron beam system developed for this program is shown in Fig. 4. All electrodes are constructed of molybdenum, since that substance has been found to be superior to any known material for use in low energy electron guns. The electrode assemblies for the electron source and monochromator (M), the electron collector (A), and the ion extraction system (S) are supported from, and precisely located with respect to each other by, a massive, carefully machined molybdenum block (2x2-1/4x2-3/16 in). Electrodes are 1.00 in dia and 0.040 in thick. The trochoidal deflection plates are actually a split cylinder of length 0.75 in and spacing 0.125 in. Support and alignment of the electrodes are provided by precision 1/16 in sapphire balls resting in locating holes. Not shown in the figure is the quadrupole mass spectrometer, which mounts on the last electrode of the ion extraction system.

Hole sizes for electrodes in the monochromator and collector assemblies are given in Table 2. Electrodes are numbered in sequence from the filament (M4, M5 and A5, A6 are split cylinder halves). The split cylinder in the collector

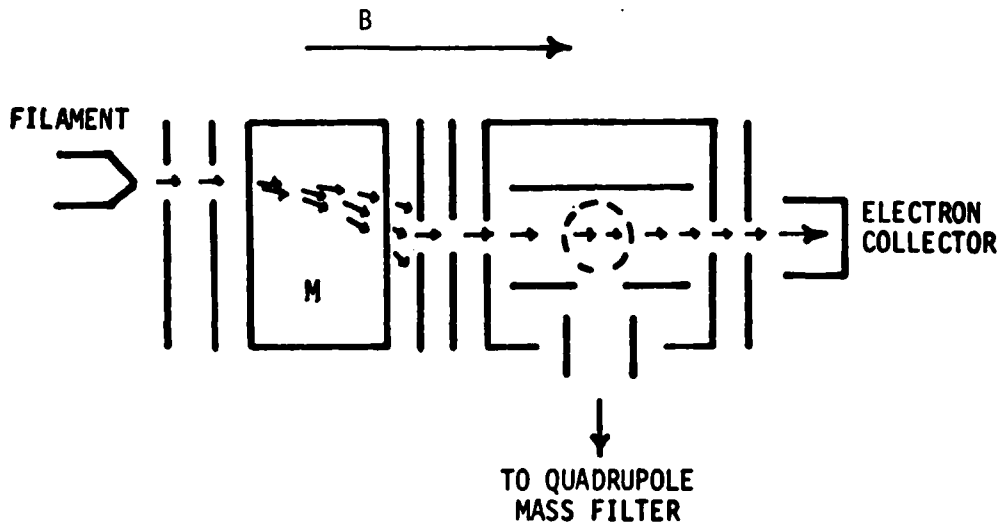

Figure 3. Schematic diagram of electron beam system. For simplicity, some electrodes are not shown.

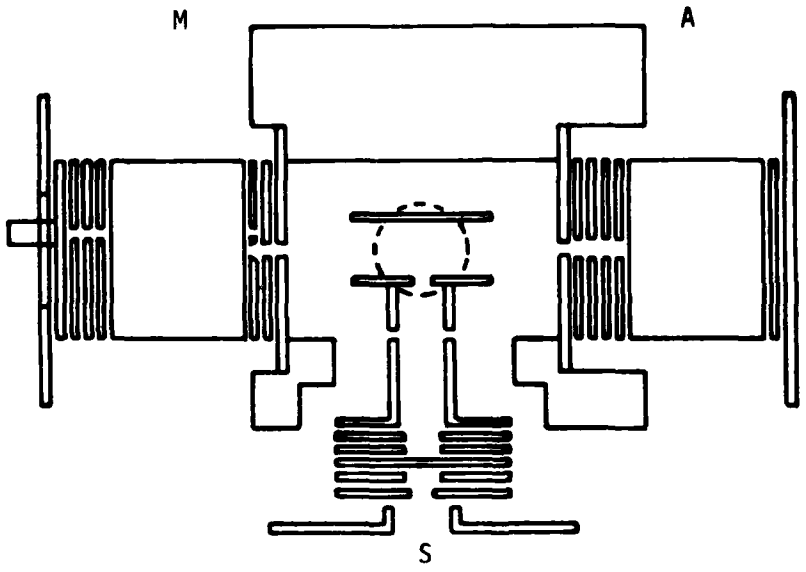

Figure 4. Scale drawing of electron gun electrode arrangement. For clarity, support structures are not shown

section acts as another trochoidal deflector and was added to keep reflected electrons from reentering the collision chamber (CC). In the collision chamber, ions are extracted by a small electric field between two parallel plates (0.8x0.4 in) through a 0.060 in dia hole in the S section. The ion extraction section contains two sets of split plates for ion deflection and steering. Dimensions are not given for the S-section since that has been replaced by a much simpler configuration in which ions are extracted along the molecular beam. The quadrupole mass filter has 0.25 in dia by 5 in long rods. Fig. 5 shows a view of the apparatus before installation of the field coils.

Table 2

Electron Beam System

Electrode Hole Sizes

Electrode	Hole Dia (in)	
M1	0.018	(3/32 in offset from axis)
M2	0.018	(3/32 in offset)
M3	0.018	(3/32 in offset)
M6	0.025	center (beveled)
	0.020	offset
M7	0.035	
CC Entrance	0.052	
CC Exit	0.062	
A1	0.067	
A2	0.070	
A3	0.073	
A4	0.073	
A7	Blank	

In all applications of trochoidal monochromators by other research groups, the device has been placed in vacuum systems composed of stainless steel tubing with fairly small diameters so that external coils could be used for production of the magnetic field. This was considered necessary because careful alignment of the magnetic field is fairly critical for proper operation of the monochromator. For the present application, the entire electron beam system, including the field coils, had to be inside the main chamber of the molecular beam apparatus. This requirement imposed severe constraints on the size and configuration of the coils.

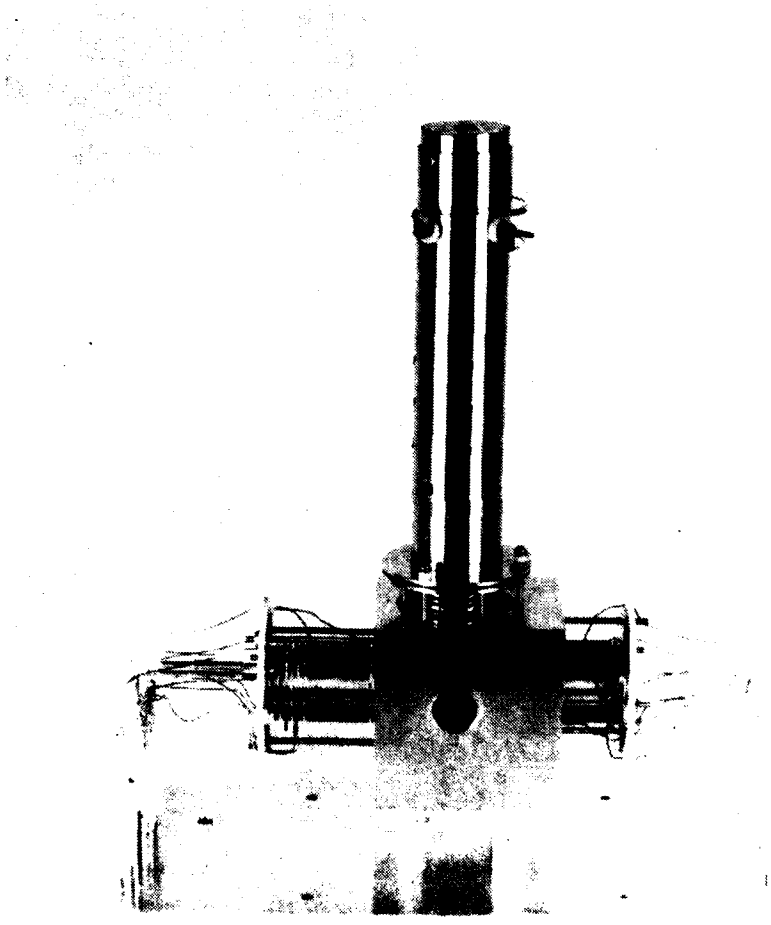

Figure 5. Electron beam system before installation of magnetic field coils and electron multiplier assembly.

It was decided to try careful geometrical alignment of the coils with the axis of the monochromator and to trim the field, if necessary, with large coils outside the vacuum system. This scheme worked well. The field coils are potted solenoids, each 4 in OD x 1.75 in ID x 1.5 in long. They slip over the M and A sections, resting against the molybdenum block, and are held in precision mountings.

The problem of supplying proper potentials to all the electrodes of a high resolution electron gun is often nontrivial. Not only must the potentials be continuously variable, but they must also be very stable and free from noise and transients. The usual method of supplying the electrodes is to use precision ten-turn potentiometers connected across one or more regulated power supplies or batteries. To avoid high current drain on the supplies, the total resistance of each potentiometer must be reasonably high - thousands of ohms or more. The leads to the electrodes are thus at fairly high impedance and must be carefully shielded. Even much care devoted to shielding does not always lead to freedom from pickup on the leads. The result of such pickup is usually degradation of the resolution and noise in the detected (ion) signals.

In an attempt to reduce this problem, the potential supply for the electron monochromator was constructed with operational amplifiers driving most of the electrodes. The basic scheme is shown in Fig. 6(a). A precision potentiometer drives the op amp (in a unity gain, non-inverting configuration) which in turn supplies the electrode at very low impedance. The arrangement in Fig. 6(b) was used to drive electrode pairs (such as deflection plates) where the potential difference ΔV between the electrodes was desired to remain fixed as the mean potential V of the pair is varied. Use of LM324 quad op amps led to a very compact and easily shielded supply. The concept of low impedance supplies to avoid pickup appears to have worked very well for this application.

Performance of the electron beam system has been excellent. A resolution of 0.02-0.05 eV FWHM is obtained with beam currents up to 1×10^{-8}A or greater. Operation down to essentially zero electron energy (< 0.05 eV) with constant beam current is easily achieved. Overall performance appears to be at least as good as the best reported in the literature.

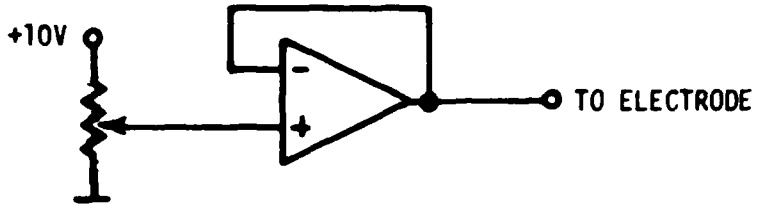

(a)

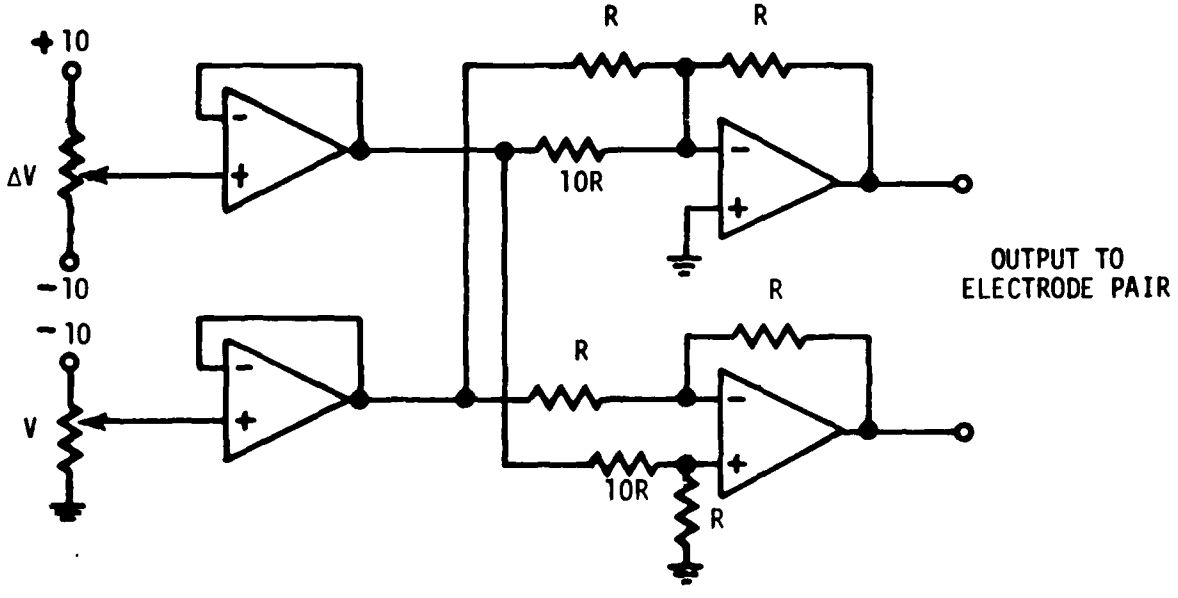

(b)

Figure 6. Typical operational amplifier circuits for driving electron beam system electrodes

It was anticipated that rf pickup problems would be experienced in operating the quadrupole mass filter so close to the electron beam system, especially in view of the rather high rf voltages required for the ion masses of interest in the program. This was indeed the case. With careful attention to grounding and shielding, however, the rf pickup was reduced to negligible levels for mass numbers less than 1000.

A channeltron electron multiplier is used for detection of ions that have passed through the mass filter. The ion detection electronics is usually operated in a synchronous detection mode with the modulated molecular beam. A system for asynchronous pulse counting was also assembled and has been used on occasion during the program. Although equipment was available for development of a synchronous pulse counting system, such a scheme was unnecessary for the investigations within this program.

3. EXPLORATORY EXPERIMENTS

During the first year of the program, an exploratory experiment was performed on H_2WO_4 and tungsten oxides using the ionizer and magnetic mass spectrometer. The purpose of this experiment was a) to develop a molecular beam apparatus and beam sources for subsequent studies, and b) to obtain crude attachment measurements for use in planning a more refined experiment. The attachment measurements were to be done with high electron beam current and, consequently, poor energy resolution, in order to determine some of the characteristics of the attachment in the tungsten compounds.

The first compound scheduled for study was H_2WO_4, tungstic acid. This species was of interest because flame studies by other investigators had indicated that the rate for the dissociative attachment reaction $e^- + H_2WO_4 \rightarrow HWO_4^- + H$ may be very high with nearly thermoneutral energetics, and that the electron affinity of HWO_4 may be large (> 4 eV). Since these observations were made at high temperatures, applications were anticipated to the engineering of combustion plasmas. Interpretation of the results of flame experiments is often difficult, so that a beam type experiment would be necessary for more definitive information.

It was originally thought that a suitable beam of H_2WO_4 could be produced by heating WO_3 powder and H_2O vapor to 1400-1600K in an inert Knudsen cell. However, a simpler method of introducing H_2O vapor into a hot tungsten Knudsen cell was tried first and was successful. A reasonable beam of H_2WO_4 was produced at oven temperatures of 1300-1700K and H_2O vapor pressures in the gas introduction system of a few hundred millitorr. Other species observed in the beam, in order of decreasing abundance, were H_2O, WO_3, $(WO_3)_3$, $(WO_3)_2$, and $(WO_3)_4$. At temperatures above 1650K, the WO_3 positive ion current, and estimated abundance, was higher than that of H_2WO_4. Estimated abundances were in at least qualitative agreement with values calculated from JANAF thermochemical data.

To obtain data on attachment in H_2WO_4, the ionizer-mass spectrometer system was set up for analysis and detection of negative ions by changing the appropriate potentials. The electron energy resolution and beam control were very poor at the necessary low electron accelerating voltages, but were sufficient for crude attachment measurements. Sensitivity for negative ions was good because of the high electron current (normally 1 μA or greater).

The most abundant negative ions observed with the (composite) H_2WO_4 beam of electron energies of 0-20 eV were WO_3^- and $(WO_3)_2^-$, although some HWO_4^- ions were present. The cross sections for production of WO_3^- and $(WO_3)_2^-$ appeared to peak at or near zero electron energy, but the HWO_4^- production seemed to onset at about 2 eV. Actual magnitudes of the WO_3^- and $(WO_3)_2^-$ currents were comparable to WO_3^+ and $(WO_3)_3^+$ currents observed for 50-100 eV electron energies, indicating that the attachment cross sections may be greater than the cross sections for positive ionization in the appropriate parent species ($1.7x15^{-15}$ cm^2 for ionization of W_3O_9). The cross section for $e^- + H_2WO_4 \rightarrow HWO_4^- + H$ appeared to be at least a factor of ten smaller than that for reactions leading to WO_3^- or $(WO_3)_2^-$.

Since attachment reactions of high cross section appeared to be associated with WO_3 and its polymers, some further studies were made using a beam of $(WO_3)_3$ and WO_3, generated by introducing pure O_2 into the tungsten oven beam source. (A small amount of $(WO_3)_2$ and higher polymers, characteristic of the equilibrium vapor of WO_3 at 1300-1800K, was also present in the beam.) The abundance ratios of species in the beam were varied by adjustment of the source temperature. The WO_3^- and $(WO_3)_2^-$ negative ion currents both appeared to vary directly as the $(WO_2)_3$ density in the beam (as determined by the $(WO_3)_3^+$ current at higher electron energies). Thus, these investigations seemed to indicate that the reactions responsible for WO_3^- and $(WO_3)_2^-$ are $e^- + (WO_3)_3 \rightarrow WO_3^- + (WO_3)_2$ and $e^- + (WO_3)_3 \rightarrow (WO_3)_2^- + WO_3$. It appears likely that electron attachment observed previously in flame studies (Ref. 3) may have involved polymers of WO_3 rather than H_2WO_4 as assumed.

Since the attachment in WO_3 vapor appeared to be more interesting than that in H_2WO_4, it was decided to pursue the former with the trochoidal monochromator, which was being built during these exploratory experiments.

4. INITIAL HIGH RESOLUTION EXPERIMENTS

During the second year of the program, studies of SF_6, WO_3 and its polymers, MoF_6, and WF_6 were made using the trochoidal monochromator apparatus. SF_6^- production from SF_6 was at first used as a check on performance of the monochromater-quadrupole system. Measurements of SF_6 attachment have been performed by several workers, so that many characteristics of the process are usually considered to be well known. The cross section for SF_6^- formation is assumed to be essentially a delta function at zero electron energy, so that the electron energy dependence of the measured cross section would simply be the energy distribution of the electron beam. During these diagnostic studies, very little attention was paid to the SF_5^- formation, other than qualitatively verifying the temperature dependence at zero energy. (Although details of the temperature dependence were not in the literature at that time, a brief description existed in the abstracts of the Gaseous Electronics Conference.) As measurements progressed in the other gases, the suspicion developed that the ion extraction geometry was strongly influencing the data, since most of the attachment observed had energy dependences similar to that of SF_6^-. In the third year of the program, the suspicion deepened as more careful studies on SF_6 yielded much smaller SF_5^- signals in the 0.1 to 1 eV electron energy range than would have been expected from the results of other workers.

Extraction of ions from the collision region in an electron beam apparatus always presents problems. Since a magnetic field is used for collimation of the electron beam, and since the ions must therefore be extracted transverse to that field, the ion paths are curved with a radius of curvature that depends on the ion energy and the field strength. The paths are also strongly influenced by electric fields used for ion drawout. With a sufficiently high drawout field, the trajectories are almost straight and efficient extraction can be accomplished through a hole somewhat larger in extent than the width of the electron beam (provided that the initial kinetic energies of the ions are low). There is,

however, a major limitation on the magnitude of the drawout field that can be used without significantly broadening the electron energy distribution in the beam. For example, in the present apparatus the diameter of the electron beam is at least 1 mm, and the spacing between the drawout plates is 8 mm. The potential drop across the electron beam in the beam intersection region is thus one eighth the potential difference between the plates (ion drawout potential). This potential drop adds directly to the energy spread in the beam; e.g., if the drawout field is 0.2 V/cm, the beam energy spread is increased by 0.025 eV.

Typically, a drawout field of 0.2 to 0.3 V/cm was used in the initial high resolution experiments. At that level, the ion extraction efficiency can be expected to be poor. Measurements of attachment cross sections vs electron energy are only meaningful if the extraction efficiency for a given ion species is constant with electron energy. This is always assumed to be the case in such experiments, although it almost certainly is not true where significant initial ion kinetic energy is involved, e.g., for many dissociative attachment processes. At low drawout fields, the extraction efficiency will also be different for different ion species, leading to errors in the determination of relative cross section magnitudes.

In the present case, the magnitudes of the SF_6^-, $MoOF_4^-$, and WO_3^- ion currents observed near zero electron energy indicated that the extraction efficiency was good at such low energies. The small SF_5^- currents observed above 0.2 eV suggested that the extraction efficiency was dropping drastically above 0.1 eV. After careful studies of the ion currents as functions of drawout potential and electron energy, it was concluded that the problem resulted from a shift in the position of the electron beam at low energies. As the beam energy approaches zero, the electrons deflect in a direction parallel to the drawout plates due to $\vec{E}x\vec{B}$ drift (where $\vec{E}$ is the drawout field). The amount of drift is proportional to the amount of time the electrons spend in the region between the plates and thus increases as the energy decreases. For the particular fields used, the drift was toward the molecular beam source.

It is apparent, then, that a geometry that is optimum for ion extraction with nearly zero energy electrons can be very poor at higher energy (at least for the parallel plate system as considered here). It should be noted that

a virtually identical geometry has been used by other investigators (Ref. 4), although apparently at higher electron energy where the $\vec{E}x\vec{B}$ drift is negligible.

Such a variable extraction efficiency obviously affects the observed width of the SF_6^- peak, thus limiting the utility of that width as a measure of the electron energy resolution. Indeed, rather poor correlation was found between the observed SF_6^- width and the width of electron beam retarding curves performed in the collision chamber (which are integrals of the electron energy distribution). On occasion, SF_6^- widths of 0.025-0.03 eV were found where 0.04-0.05 eV would be expected with 0.02 eV basic resolution plus broadening by the drawout potential.

After it was discovered that the extraction geometry was not acceptable, the quadrupole mass filter was removed from the ion extraction assembly and placed in the plane of the two beams near the exit of the molecular beam from the collision chamber, at an angle of 55° to the molecular beam. Ions were extracted from the collision region along the molecular beam and steered into the quadrupole mass filter with a set of curved electrostatic deflector plates. This arrangement performed very well, apparently eliminating many of the extraction problems. It should be noted that energy analysis of the ions can be done with the electrostatic deflector, although little use was made of this feature during the present program.

Data on energy dependences of attachment taken with the original extraction system are obviously not valid. (However, in those cases that have been checked, relative magnitudes of cross sections for different ion species compared at the same electron energy appear to be in reasonable agreement with those measured with the new extraction system.) The remainder of this section will thus be devoted to only a brief description of the initial experiments that were performed during the second year of the program.

After "diagnostic" studies with SF_6, measurements were begun on WO_3 and its polymers with the high resolution apparatus. At first a tungsten foil oven beam source was used, as in the exploratory experiments of the first year. Oxygen was flowed through the oven, so that WO_3 vapor (composed of $(WO_3)_n$, n = 1,2,3, and other polymers) was formed for temperatures above 1400K. Fairly good WO_3^- signals were observed, but the beam density varied so rapidly with time that measurement of the energy dependence of the cross section was not possible. Oven lifetime was about two hours, so that several oven configurations were tried

in attempts to achieve a stable beam and long oven life. Finally, an oven was constructed of iridium, sapphire, and tungsten that yielded a reasonably steady beam of tungsten oxides. Beam intensities were not strong, and became weaker with time, but the oven was not subject to failure.

Data on attachment in $(WO_3)_n$ were shown in the annual report for the second year of the program. That information is not reproduced here because it was obtained with the old ion extraction system. Evidence to support our hypothesis that the major attachment reactions are $e^- + (WO_3)_3 \rightarrow WO_3^- + (WO_3)_2$ and $e^- + (WO_3)_3 \rightarrow (WO_3)_2^- + WO_3$ is provided by recent plasma quench investigations with tungsten oxide (Ref. 5).

The investigations of attachment in MoF_6 and WF_6 near the end of the second year of the program were inspired in part by a need within the Air Force for basic data on these compounds. Results of our initial studies were presented in a report (IRT 8164-002), the major portion of which is reproduced in Appendix B. Although the data for that report were taken with the original extraction system, most of information derived therefrom seems to be valid. $MoOF_4^-$ does appear to be essentially a zero energy peak, but the energy dependence of MoF_6^- has since been found to be quite different. The initial study thus complements the later work presented in Section 5.

5. THIRD YEAR EXPERIMENTAL RESULTS

5.1 SULFUR HEXAFLUORIDE

After the ion extraction problem had been found and corrected, a detailed study of attachment in SF_6 was performed. Although many workers have investigated SF_6 attachment with both electron beams and swarms, there remain inconsistencies between the various results and some unanswered questions. The present experiment is the first to use crossed beams and probably has the highest energy resolution of any comprehensive investigation.

Electron attachment to SF_6 in the 0-1 eV electron energy range is considered to occur through the reactions

$$e^- + SF_6 \rightarrow SF_6^- \qquad \text{(direct attachment)}$$

and

$$e^- + SF_6 \rightarrow SF_5^- + F \qquad \text{(dissociative attachment)} .$$

The SF_6^- ion formed in direct attachment is metastable with a lifetime that probably depends upon the internal energy state of the SF_6 target molecule and the energy of the incident electron. (In swarm or flowing afterglow experiments, the SF_6^- ions are stabilized by collisions with the background gas.) The direct attachment cross section has been thought to be essentially a delta function at zero electron energy (< 0.003 eV width according to W. Chupka, unpublished measurements), but one recent study (Ref. 6) with threshold photoelectron spectroscopy finds a FWHM of 0.033 eV. Some metastable SF_6^- has been observed by several investigators to decay into SF_5^-. (The other mode of decay is autoionization.) This observation would indicate that at least some of the SF_6^- is formed in a temporary state lying above the SF_5^--F dissociation limit.

Typical present measurements on SF_6^- formation as a function of electron energy are shown in Fig. 7. The zero of the electron energy scale has been set approximately to the energy of the cross section peak. The energy width of the SF_6^- curve is about 0.05 eV FWHM, and this value is typical for data taken after modification of the ion extraction system. Electron beam retarding curves

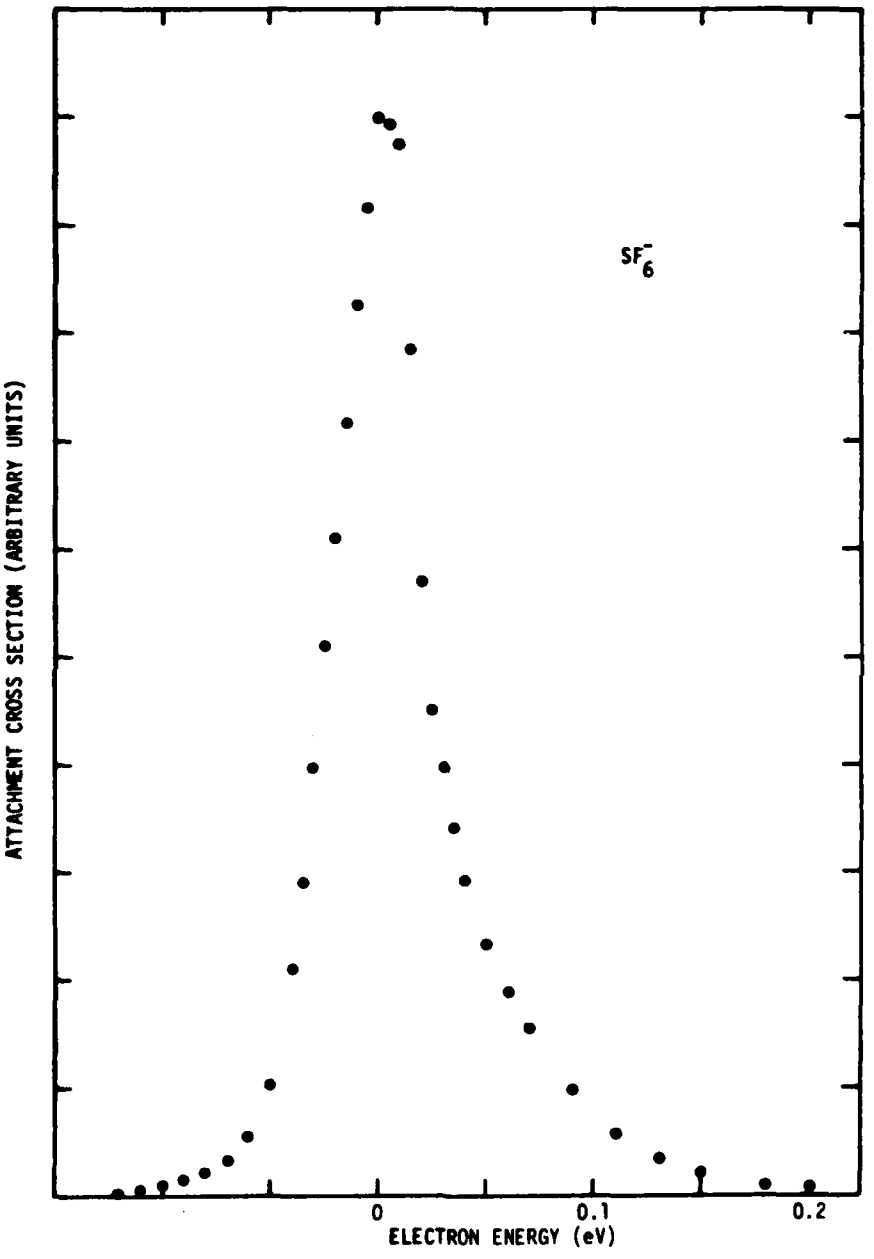

Figure 7. Cross section for SF_6^- at room temperature

indicated that the energy resolution may have been on the order of 0.02 eV for much of the data. If this was indeed the case, it would imply an intrinsic width for the SF_6^- cross section of about 0.03 eV under the conditions of this experiment (temperature and ion flight time). The width is observed to decrease slightly with increasing SF_6 beam source temperature, and this may also indicate that the measured SF_6^- FWHM was not merely reflecting the FWHM of the electron beam energy distribution.

The peak magnitude of the SF_6^- cross section decreases rapidly with increasing molecular beam source temperature. A new observation here is that the tail of the cross section (i.e., the cross section in the region above 0.05 eV) decreases more rapidly than the peak with temperature. (At room temperature, the SF_6^- cross section is found to decrease exponentially with increasing energy. An e-folding energy of 0.04 eV was observed, in excellent agreement with the value of 0.043 eV given in Ref. 1.) This is interpreted as probably due to a shorter lifetime of SF_6^- formed with electron energies greater than 0.05 eV when the SF_6 target has higher temperature (greater internal energy). Quantitative comparison of these data with theory will be made when a unimolecular decay theory for SF_6^- is available (presently being developed by Dr. K. Westberg of Aerospace Corporation).

The dissociative attachment process, $e^- + SF_6 \rightarrow SF_5^- + F$, exhibits several interesting features. Figure 8 shows our measurements on SF_5^- for molecular beam source temperatures of 296K, 352K, and 386K, together with an arbitrarily normalized SF_6^- curve for comparison. Source temperatures were measured with a Pt-Pt +10% Rh thermocouple attached to the source oven. At higher temperatures, the zero energy peak becomes extremely large, the tail blending into and obscuring the higher energy peak. The zero energy peak is virtually nonexistent below 290K.

The form of the SF_5^- cross section in the temperature range 300-400K would suggest that there are two distinct processes leading to SF_5^- formation. The zero energy peak probably arises from decay of SF_6^-, the rapid growth of the tail with temperature resulting from the enhanced decay above 0.05 eV. The higher energy process, peaking at 0.5 eV at room temperature, has a more modest temperature dependence, exhibiting a shift of the cross section peak to lower energies with increasing temperature as well as an increase in magnitude.

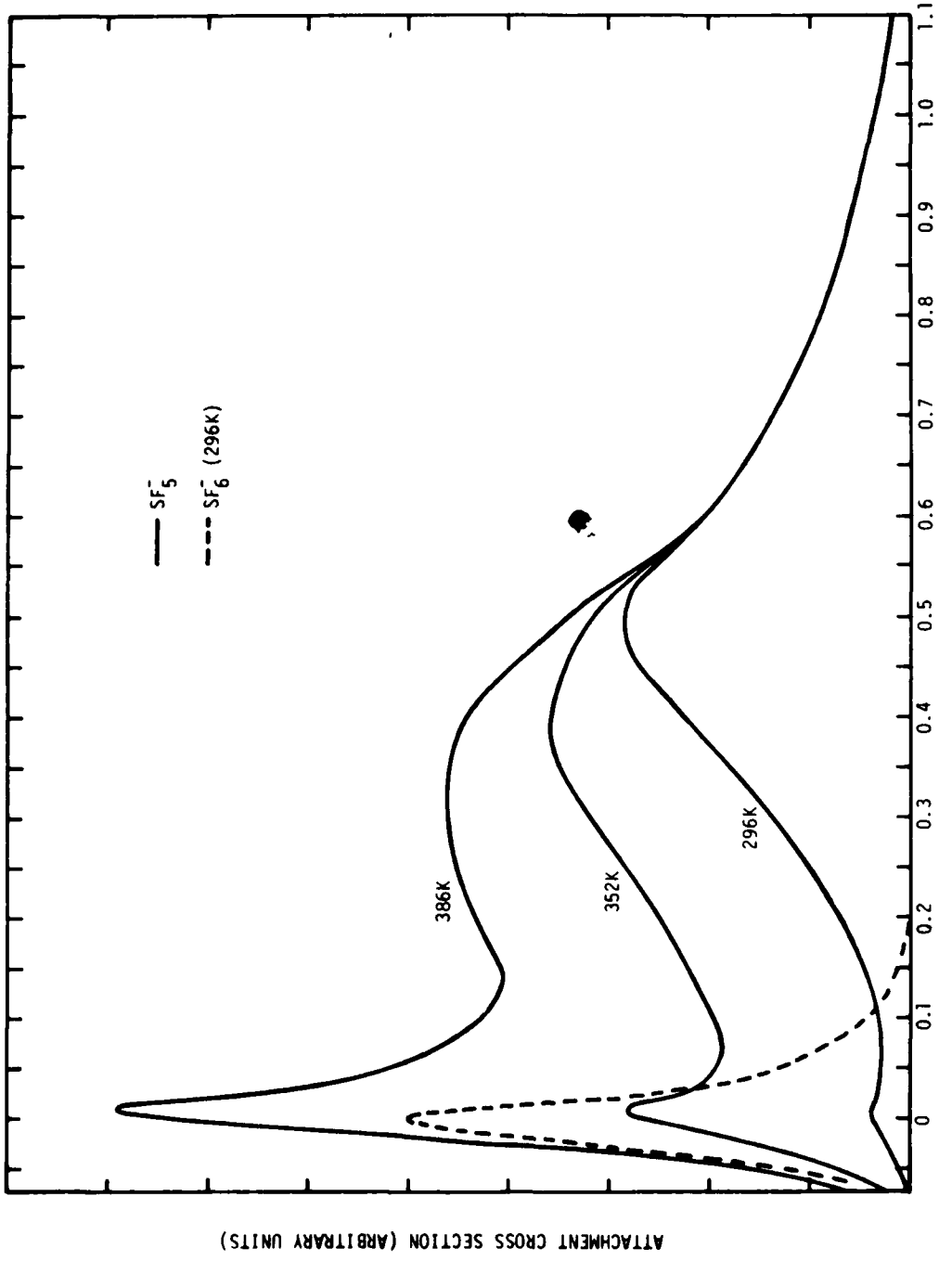

Figure 8. Cross section for SF_5^- formation vs electron energy at three beam source temperatures

While these measurements were being taken, the results of Chen and Chantry (Ref. 8) on SF_5^- became available, allowing comparison of data from a somewhat different type of apparatus. In their case, the electron beam passes through a heated gas cell instead of a molecular beam. The flight time of the ions is probably nearly the same in the two experiments. The cross section curves are very similar to those of Fig. 8, except that their 300K curve corresponds to the shape we would observe at about 360K. There would be excellent agreement if it were assumed that their collision chamber was actually 50-60K higher in temperature than they measured. In an apparatus of that type, we have observed that the parts of the electron beam system are usually at about 360K during operation, due to heating by the filament. However, Chantry has indicated that great care was taken in their case to thermally isolate the collision chamber and that the temperature was monitored with a thermocouple. In the present case, the beam source is, of course, totally separated from the electron beam system, and careful investigations yielded no evidence that the temperature was other than what we measured.

Another point of disagreement, which may be related to the first, is in the temperature dependence of the zero energy peak over a wide temperature range. Figure 9 is a typical semilogarithmic plot of the SF_5^- cross section at zero energy vs 1/T, where T is the beam source temperature in K. Although the data points do not fit a straight line, the line shown would yield an "activation energy" of 0.34 eV. (A value of 0.35 $\pm$ 0.05 eV is found from analysis of several sets of such data.) In a similar plot, Chen and Chantry (Ref. 8) find the data points falling close to a straight line with an activation energy of 0.2 eV. If there is indeed an error in their temperature scale of the magnitude and direction suggested above, then there would probably be good agreement. In addition, if the SF_5^- near zero energy does result from decay of SF_5^-, there would be no reason a priori to expect a linear plot and unique "activation energy." Indeed, the contribution from the higher energy process should be subtracted out at the lower temperatures.

The temperature dependence of the higher energy SF_5^- peak from 300K to 400K is similar in many respect to the case of dissociative attachment in O_2 (Ref. 9). Since the O_2 work had been nicely interpreted by the theory of O'Malley (Ref. 10), it seemed that similar considerations might apply to SF_5^-.

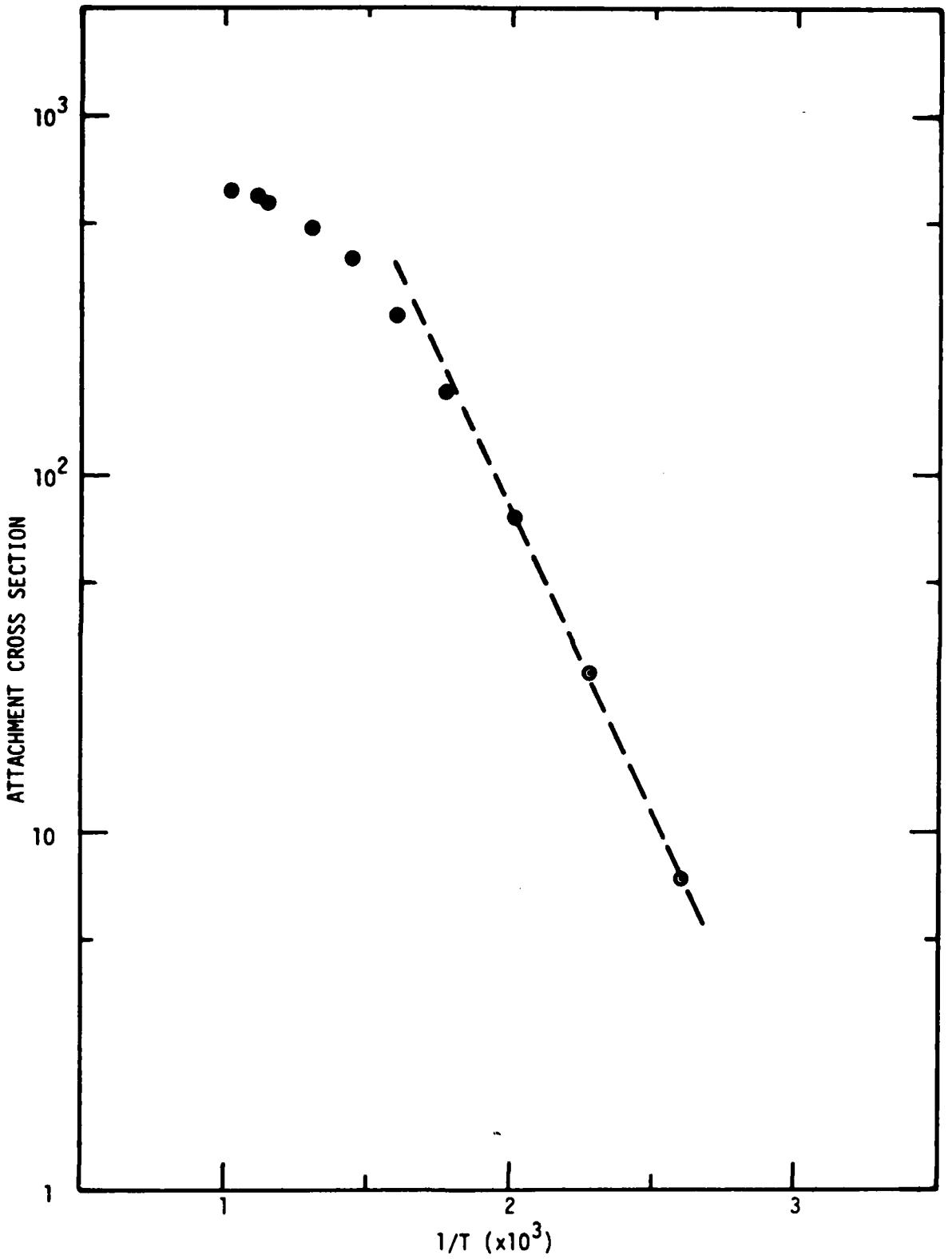

Figure 9. Semilogarithmic plot of zero energy SF_5^- cross section vs inverse temperature

In O_2, the enhanced attachment cross section and peak shift with temperature result from the increasing vibrational internal energy of the target molecules. In the case of SF_6, significant vibrational internal energy is present even at room temperature. Following the results of the theory for O_2, we investigate a possible fit of the SF_5^- data to

$$Q(E,T) = C(E)\ e^{-D(E)/kT}$$

as a form for the cross section as a function of electron energy E and temperature T. Figure 10, which is derived from the data of Fig. 8, is a sample semi-logarithmic plot of the SF_5^- cross section vs 1/T for electron energies of 0.25, 0.30, and 0.40 eV. It is seen that the points accurately fit straight lines for each electron energy. Excellent straight line fits were found with similar plots for all electron energies between 0.2 and 0.5 eV. Thus, the data appear to obey the expression above for each electron energy in that range. Upon evaluating D(E), the slope of the line for energy E, at each energy, we obtain Fig. 11, a plot of D(E) vs E. The variation of D with E appears to be linear, although this would not necessarily be expected from the theory. In the sense of O'Malley's theory, the slopes D(E) could be called activation energies, in that they are interpreted for a given E as the average internal energy that maximizes the thermal average of the cross section over the internal state population at that E.

Figure 12 shows schematic potential energy curves for the SF_6 and SF_6^- systems, assuming a "diatomic" model. $D(SF_5\text{-}F)$ is the bond dissociation energy of SF_6 (3.9 ± 0.15 eV, according to Ref. 11), and $EA(SF_5)$, $EA(SF_6)$ are the electron affinities of SF_5 and SF_6 (which are not yet known to any accuracy). The dissociative attachment process centered at 0.5 eV is usually considered to arise from a repulsive curve as shown leading to SF_5^- + F (Ref. 8). The energy balance equation for the process is

$$E = D_s(SF_5\text{-}F) - EA(SF_5) + KE\ ,$$

where E is the electron energy, KE is the kinetic energy of the SF_5^- and F fragments, and D_s is the dissociation energy for the SF_6 state involved in the attachment. A value $EA(SF_5) \geq 3.4 \pm 0.2$ eV has been obtained from dissociative electron transfer experiments (Ref. 12), which would give a nominal electron energy value for onset of dissociative attachment of ≤ 0.5 eV. Since our analysis

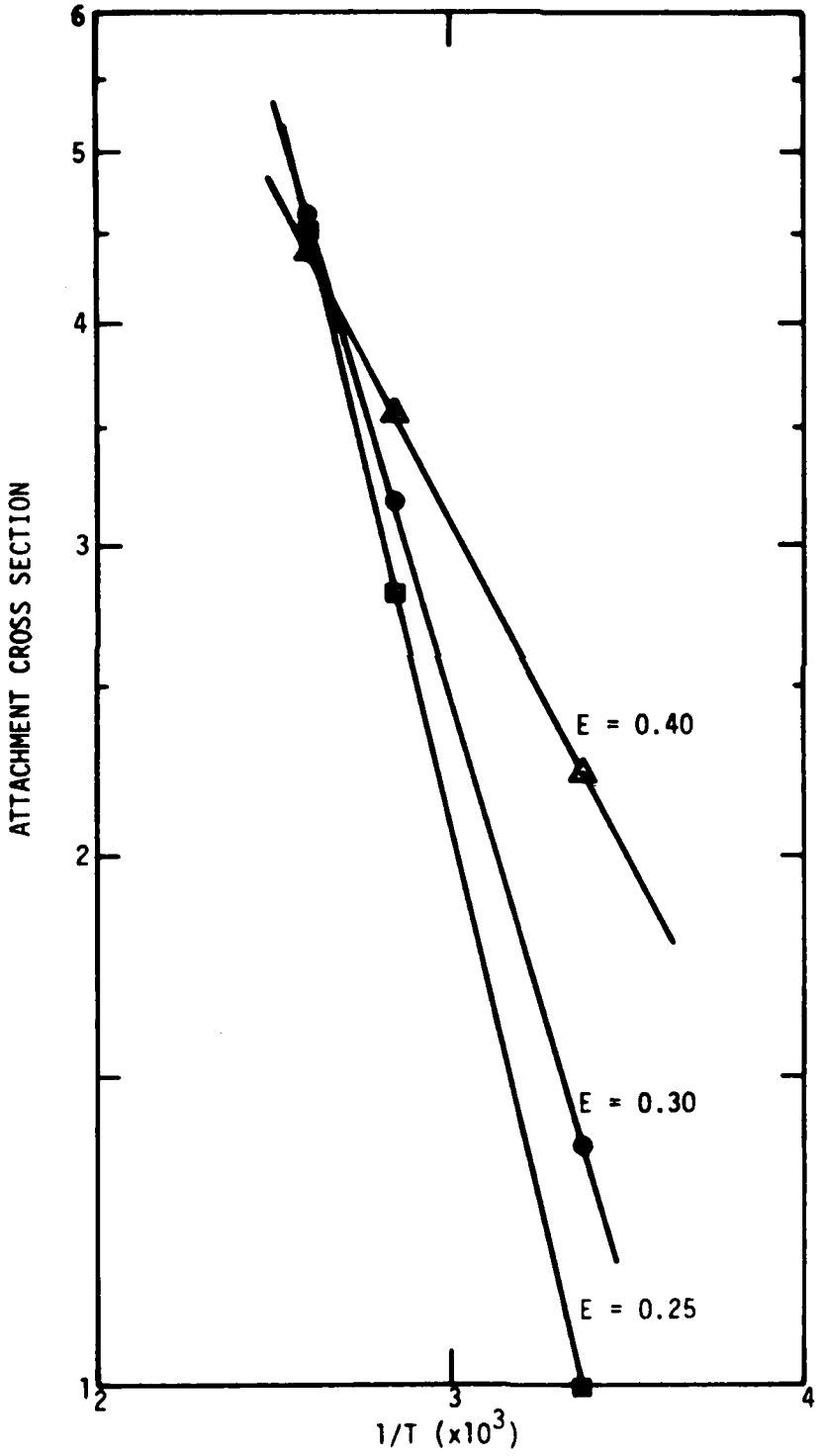

Figure 10. Semilogarithmic plot of SF_5^- cross section vs inverse temperature at three electron energies

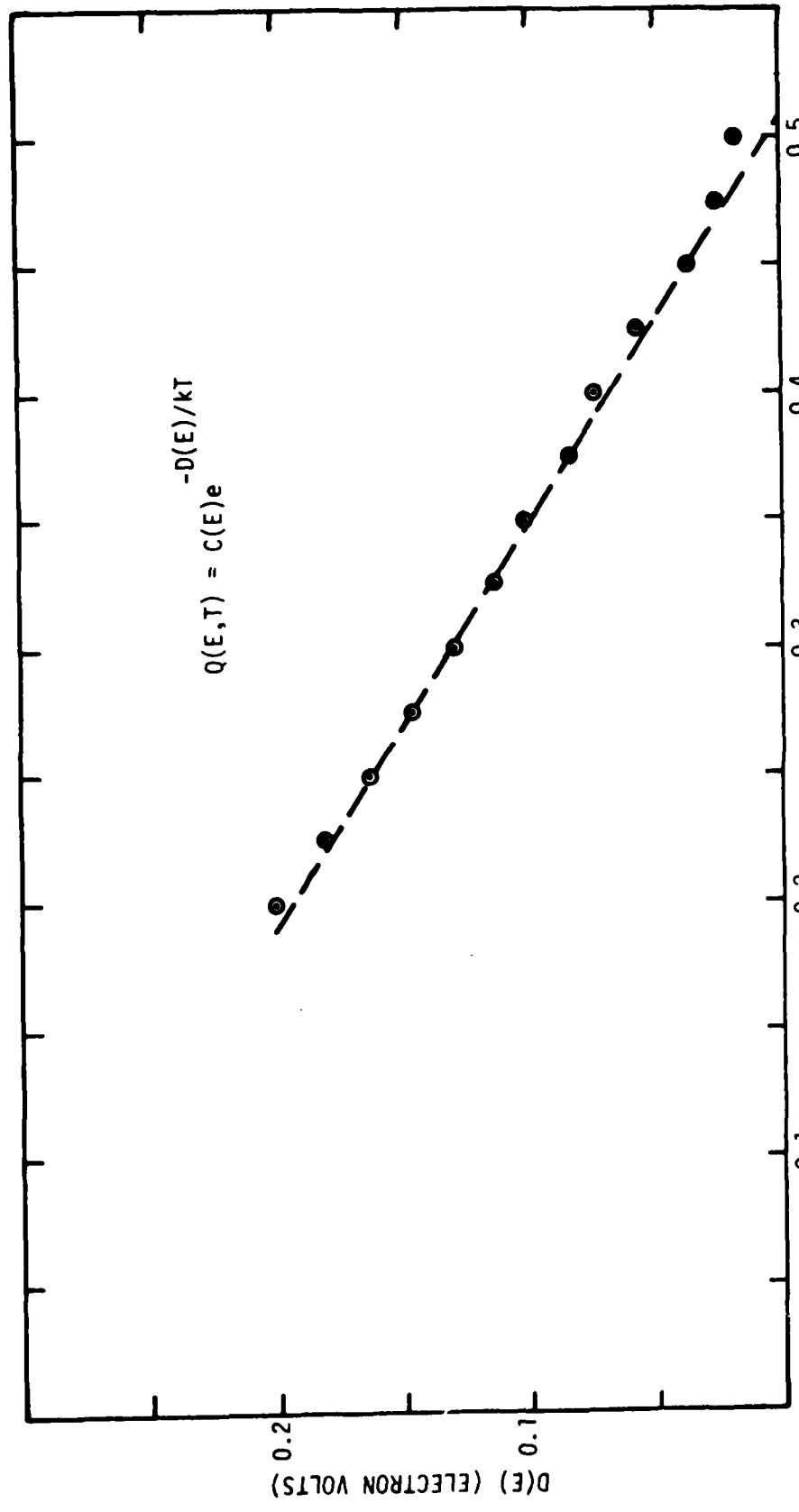

Figure 11. Plot of D(E) vs electron energy E, as derived from the data for Q(E,T) in Figure 8

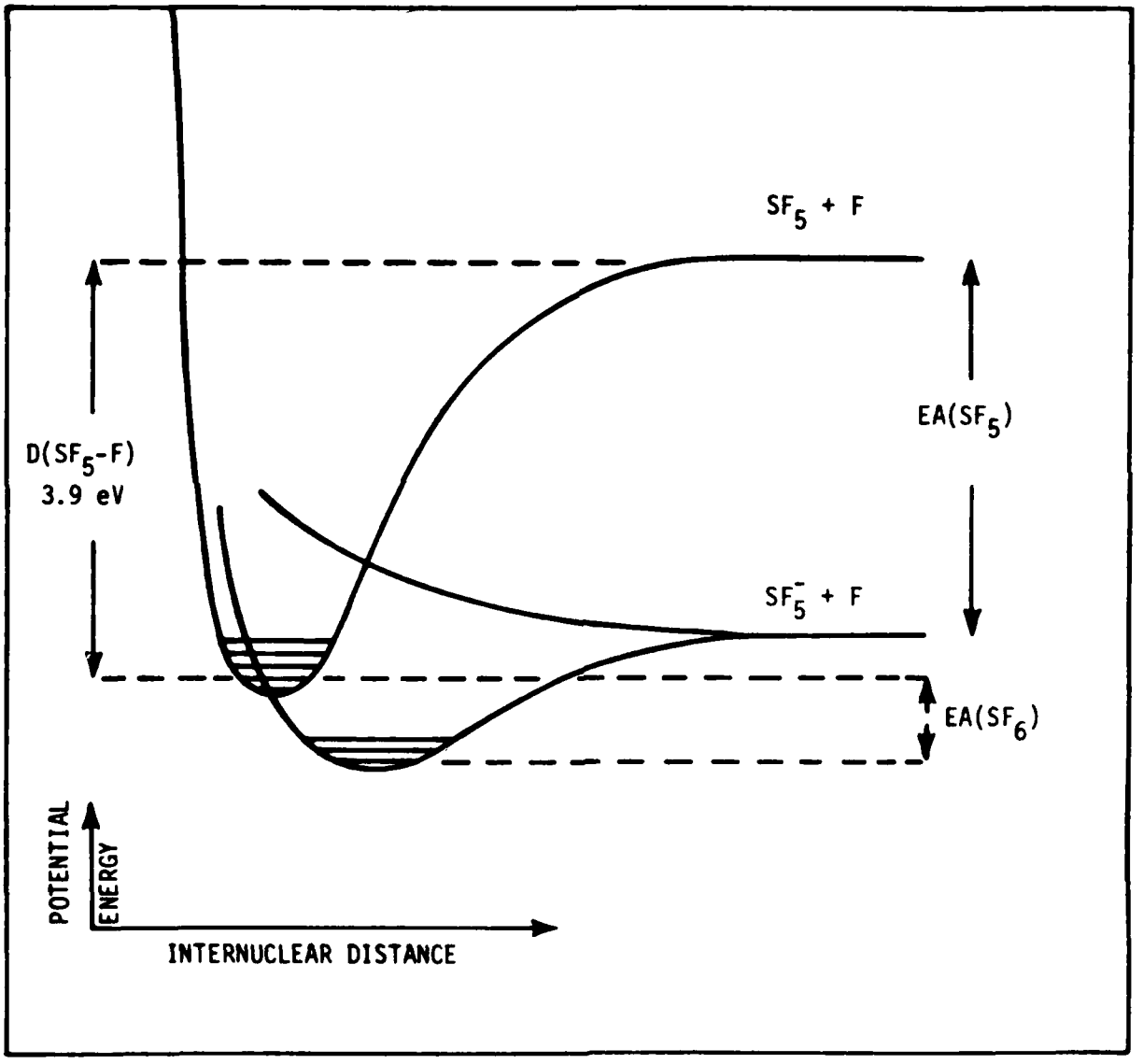

Figure 12. Schematic potential energy diagrams for SF_6 and SF_6^-

above has shown that effects of SF_6 internal energy dominate the attachment below 0.5 eV, and since the kinetic energies of the SF_5^- have not been measured, it is not possible at this time to derive a firm value for $EA(SF_5)$. Indeed, given the strong internal energy effect, the data are consistent also with an attractive SF_5^--F potential curve giving rise to the attachment. A vertical onset would be expected in that case, a phenomena that might become apparent if experiments were performed with source temperatures considerably below 300K. Because of the linearity observed in Figs. 10 and 11, it is tempting to believe that further analytical work along the lines of O'Malley's theory might yield more insight into the energetics of the dissociative attachment.

5.2 MOLYBDENUM HEXAFLUORIDE

Electron attachment in MoF_6 was reinvestigated after the change in the ion extraction system. As in our earlier studies (see Appendix B), significant attachment to $MoOF_4$ as an impurity was observed. The cross section for $MoOF_4^-$ production from $MoOF_4$ appeared to have essentially the same energy dependence as that for SF_6^- from SF_6 (Fig. 7). Detailed comparison of the tailing (0.05-0.2 eV) could not be made because of the presence of signal from MoF_5^-. Also, there was no control over the vapor pressure of $MoOF_4$ in the molecular beam source, so that more attempts at quantitative measurement were not considered worthwhile without changing over to the study of that compound alone.

In the investigation of MoF_5^- production from MoF_6 with the new extraction system, it was found that most of the dissociative attachment occurs at electron energies above 0.3 eV. Data at room temperature are shown in Fig. 13. The contribution from $MoOF_4^-$ has been removed from these data, and the cross section has thus been extrapolated for electron energies below 0.3 eV. Similar data were taken at several temperatures up to 480K. Changes in the cross section with temperature are not dramatic - a drop in peak cross section of 10-15% from 296K to 373K and only a few percent further variation up to 480K. There is evidence that the curve may involve two processes or states (as manifested by the small dip at about 0.8 eV) with slightly different temperature dependences. The cross section apparently does increase very slightly with temperature below 0.5 eV. One run was attempted at 756K, but the resulting large $MoOF_4^-$ signal caused great difficulty. The two distinct humps near the peak did disappear and there appeared to be a shift in peak cross section toward lower

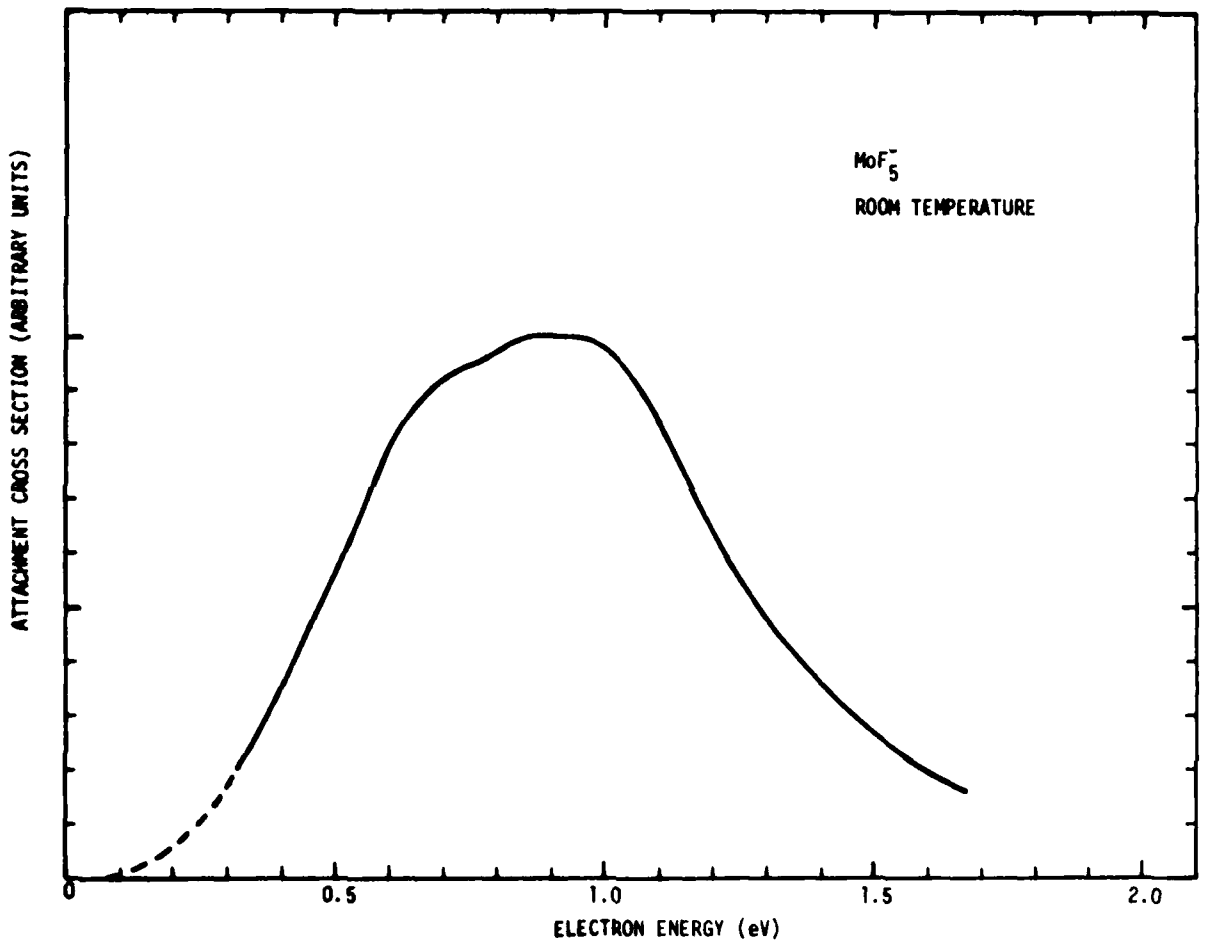

Figure 13. Cross section for production of MoF_5^- at room temperature as a function of electron energy. The dashed portion is an extrapolation

energies. The general form of the room temperature cross section above 0.5 eV agrees reasonably with that from the only previous study (Ref. 13).

The cross section for production of MoF_6^- exhibits a much more striking temperature dependence. Figures 14 and 15 show data on the direct attachment at five temperatures from ambient to about 500K. It is apparent that the peak at 0.25 eV decreases rapidly with increase in temperature, all but disappearing by 450K, whereas the zero energy peak increases slightly up to 375K, then decreases. It should be noted that the tailing of the zero energy peak at 500K is substantially larger than that of SF_6^- at room temperature. Agreement with the room temperature data of Ref. 13 for the shape of the MoF_6^- cross section is poor.

That the direct attachment in MoF_6 occurs over such a wide energy range (0.5 eV) is surprising. The apparent presence of two distinct mechanisms or pathways for the process as revealed by the temperature dependence studies is also very interesting. Unfortunately, there was not time within the present program to pursue these questions further.

5.3 TUNGSTEN OXIDE

Near the end of the program, some further data was obtained on attachment in WO_3 vapor. A new oven was constructed and a beam of $(WO_3)_n$ was produced by heating WO_3 powder. The beam was reasonably stable for periods of several hours. Again, the major component of the beam was $(WO_3)_3$. An example of the data obtained for WO_3^- is shown in Fig. 16. The curves for $(WO_3)_2^-$ were very similar. Because of insufficient time, no data was taken for electron energies above 1.5 eV, nor were the temperature dependences of the cross sections investigated. Nothing was observed that would justify further efforts on this very difficult compound, since even a complete set of data would probably not add significantly to the understanding of attachment processes.

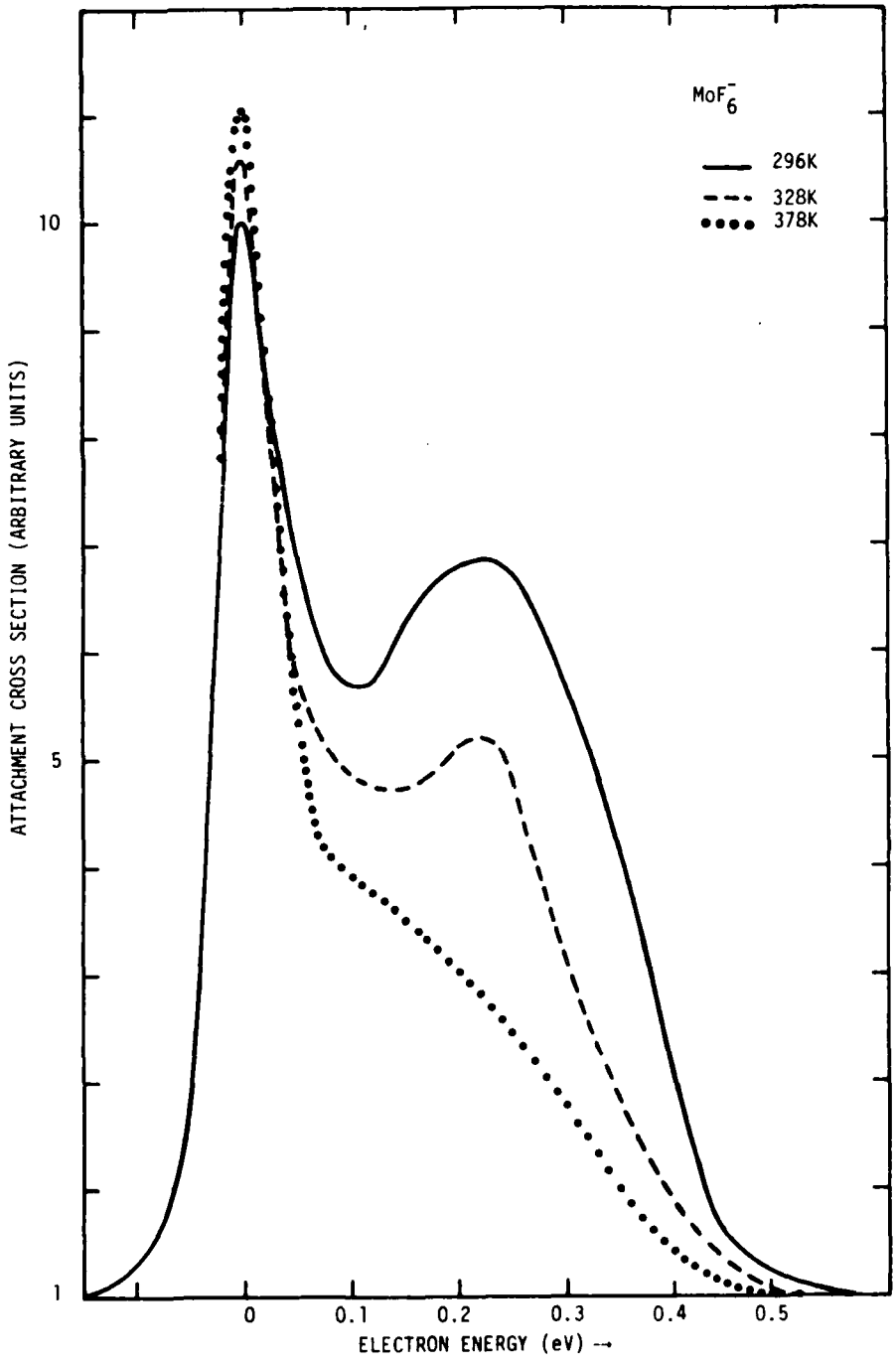

Figure 14. Cross section for production of MoF_6^- as a function of temperature

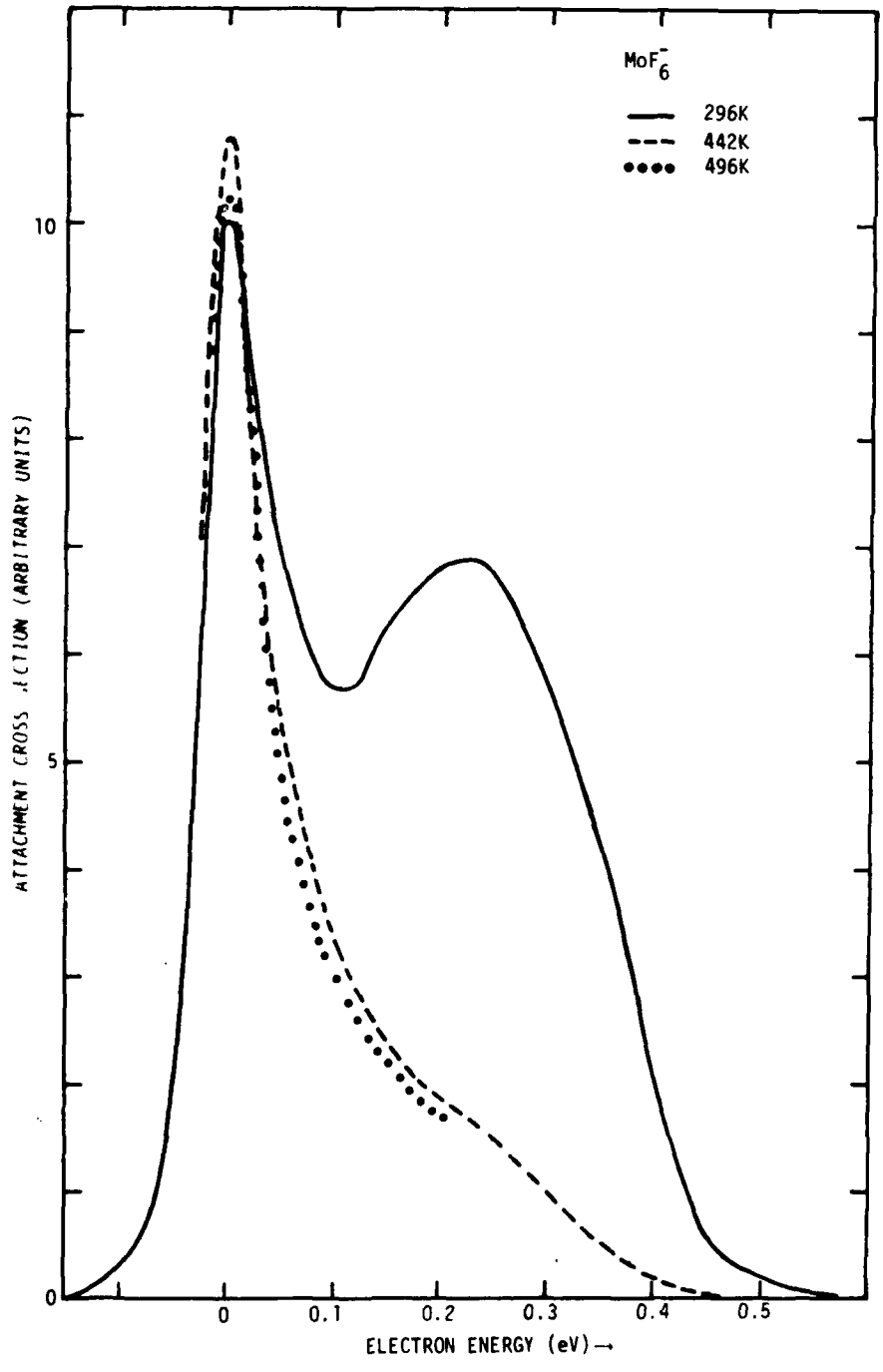

Figure 15. Cross section for production of MoF_6^- as a function of temperature

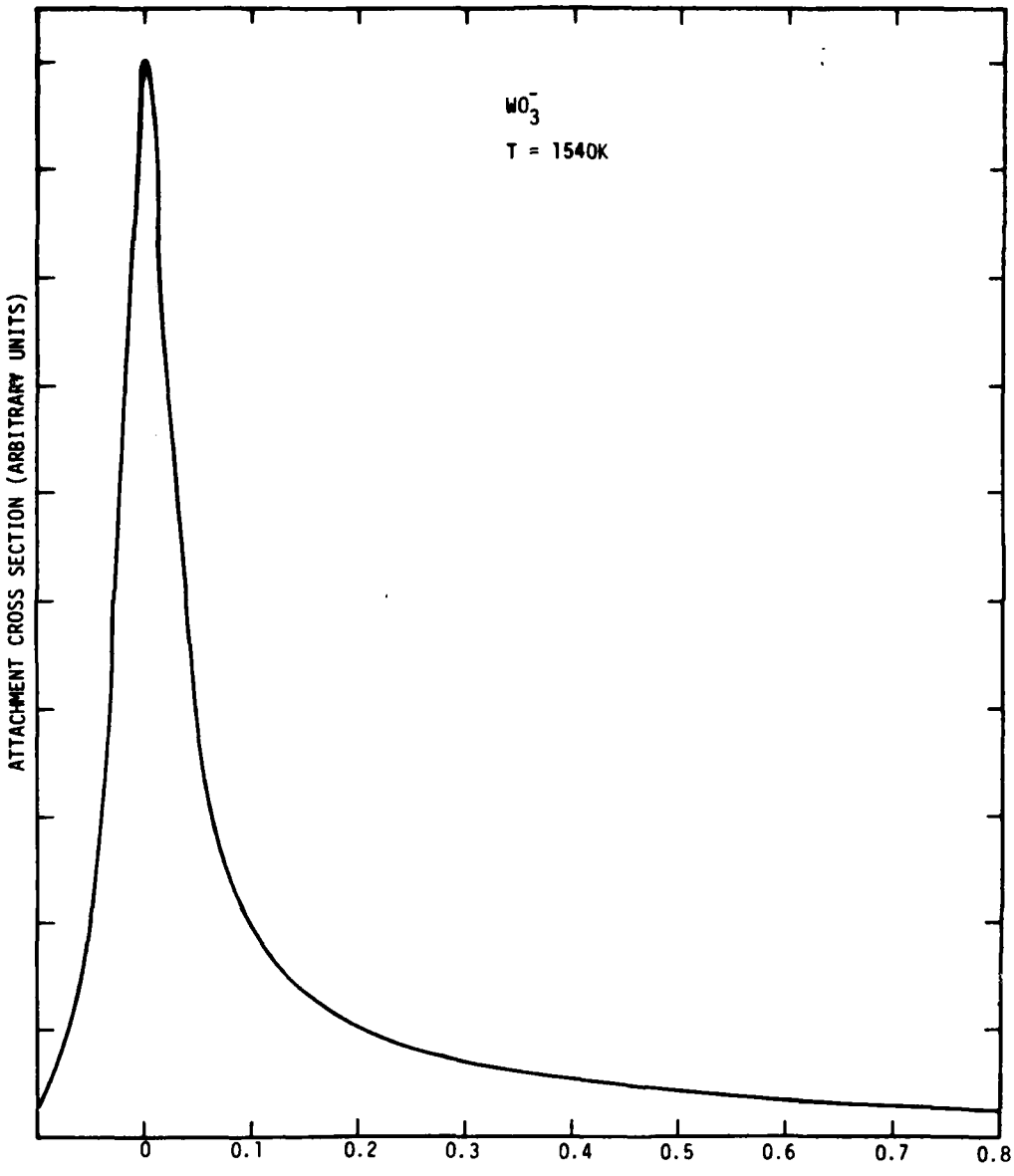

Figure 16. Cross section for production of WO_3^- at 1540K

6. SUMMARY

A crossed beam apparatus has been developed that is well suited for investigation of two-body electron attachment down to very low electron energies. Excellent electron beam energy resolution was achieved. Through variation of the target molecule temperature, it was found that internal energy plays a very important role in attachment processes for polyatomic molecules, even at room temperature. Thus, any future attachment experiments on polyatomics will have to incorporate studies of the temperature variations of cross sections was well as the features traditionally measured.

Attachment in SF_6 and MoF_6 was studied in detail in this program, and some measurements were done on attachment in the very difficult WO_3 polymer system. Some significant new results were obtained in SF_6, and it is intended that a paper on them be submitted soon to the Journal of Chemical Physics. Although not enough information is available for full interpretation of the MoF_6 data, a short paper on that material will also be submitted to the same journal. It is expected that the WO_3 work will be published as a short note in Chemical Physics Letters.

7. ACKNOWLEDGMENTS

J. A. Rutherford of IRT Corporation has contributed greatly to the program through direct work on the project and useful discussions. Dr. D. A. Vroom, Dr. S. M. Trujillo, and R. L. Palmer have also contributed through informative discussions, as have Dr. Karl Westberg (Aerospace Corporation), Prof. P. D. Burrow (University of Nebraska), Dr. P. J. Chantry (Westinghouse Research Laboratory), and J. H. Kearney (Yale University).

REFERENCES

1. For a review, see G. J. Schulz, Rev. Mod. Phys. 45, 378 (1973) and 45, 423 (1973).

2. A. Stamatovic and G. J. Schulz, Rev. Sci. Instr. 41, 423 (1970).

3. D. E. Jensen and W. J. Miller, J. Chem. Phys. 53, 3287 (1970).

4. A. Stamatovic and G. J. Schulz, J. Chem. Phys. 53, 2663 (1970); Phys. Rev. A7, 589 (1973).

5. J. M. Madson, 17th Aerospace Sciences Meeting, New Orleans, January, 1979.

6. J. M. Ajello and A. Chutjian, J. Chem. Phys. 71, 1079 (1979).

7. L. E. Kline, D. K. Davies, C. L. Chen, and P. J. Chantry, J. Appl. Phys. 50, 6789 (1979).

8. C. L. Chen and P. J. Chantry, J. Chem. Phys. 71, 3897 (1979).

9. W. R. Henderson, W. L. Fite, and R. T. Brackmann, Phys. Rev. 183, 157 (1969).

10. T. F. O'Malley, Phys. Rev. 155, 59 (1967).

11. T. Kiang, R. C. Estler, and R. N. Zare, J. Chem. Phys. 70, 5343 (1979).

12. C. Lifshitz, T. O. Tiernan, and B. M. Hughes, J. Chem. Phys. 72, 789 (1980).

13. J. A. D. Stockdale, R. N. Compton, and H. C. Schweinler, J. Chem. Phys. 53, 1502 (1970).

APPENDIX A

ATTACHMENT RATE MEASUREMENTS WITH A QUADRUPOLE ELECTRON TRAP

During the planning of the present program, a new technique was conceived for the determination of electron attachment rates over a wide range of temperature. Although this method was not used in the program (primarily because a crossed beam experiment yields information that is more fundamental), a description of the basic principles involved is presented here for future reference.

The new technique consists basically of passing a molecular beam of the species of interest through a cloud of electrons whose number is measurable. The attachment rate of electrons to beam molecules is obtained by measurement of the depletion rate of the electrons together with determination of the molecular density in the beam. The temperature of the electrons can be varied from ambient (300K or less) to greater than 10,000K and the beam source temperature can be varied independently, so that attachment coefficients can be obtained as functions of temperature over a wide range.

A Penning-style, quadrupole electron trap (Ref. A1) is used for containment of the electron cloud. Figure A1 shows a schematic diagram of the trap. The molybdenum electrodes, whose surfaces are accurately hyperboloidal, are cylindrically symmetric about the z-axis and consist of two end caps and a central ring. Application of a potential V_o to the ring with the end caps at ground yields an electrostatic saddle potential (Figure A2)

$$V = V_o \frac{r^2 - 2a^2 + 2d^2}{\rho^2 + 2d^2}$$

within the trap, where 2ρ is the equatorial diameter of the ring, $2d$ is the axial distance between the end caps, and (r,z) are cylindrical coordinates with origin at the center of the trap. (Typical dimensions are 2ρ = 1.25 cm and $2d$ - 0.76 cm.) With V_o positive, a potential well for electrons is present in the z-direction. Electrons can thus be trapped along the axis if their energies are sufficiently small compared with the well depth. Since the electrons experience a repulsive force in the radial direction, a

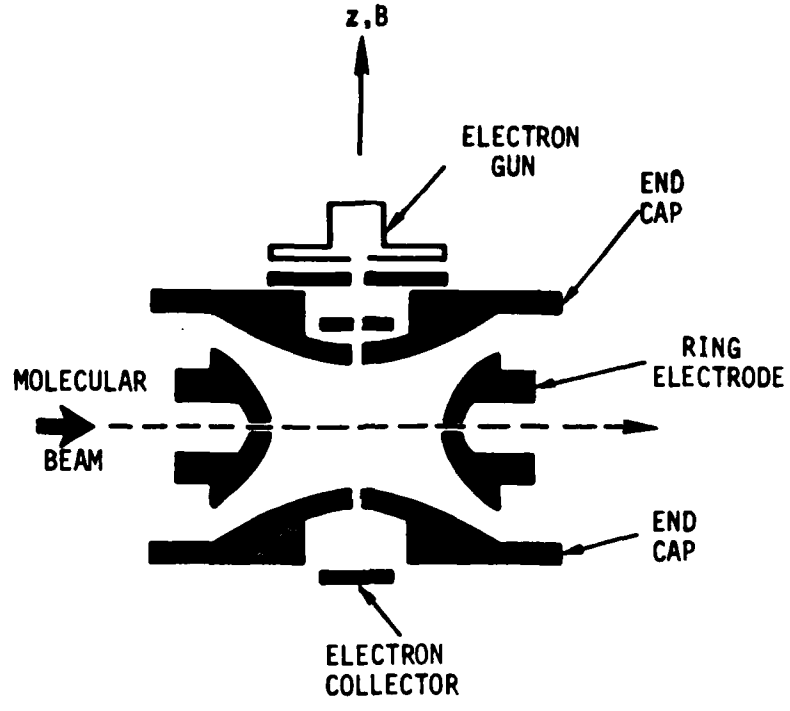

Figure A1. Schematic diagram of quadrupole electron trap. The electrodes are cylindrically symmetric about the z-axis, with exception of the molecular beam slits in the ring electrode

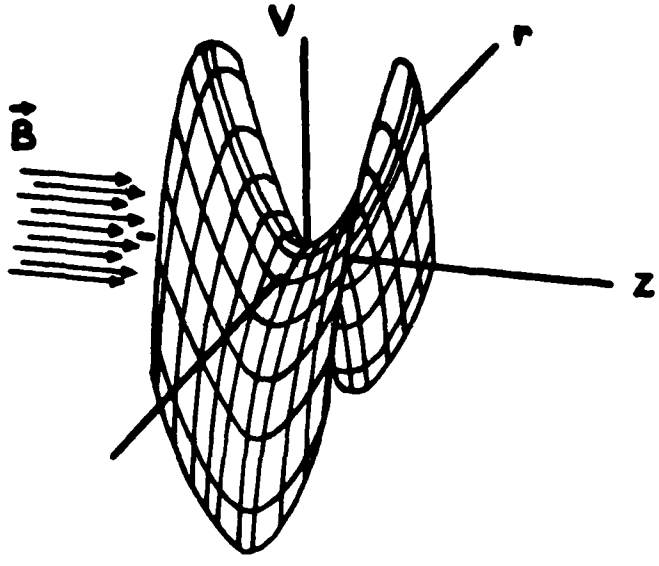

Figure A2. Form of electrostatic saddle potential in electron trap

strong, uniform magnetic field B is applied along the axis, inducing cyclotron and magnetron motion with consequent radial confinement of the electrons.

Previous workers (Refs. A1-A6) have thoroughly investigated (theoretically and experimentally) the behavior of electrons in a static quadrupole trap. Here we briefly summarize the results. The motion of the electrons is a superposition of three separate motions: (1) harmonic oscillation parallel to the z-axis, (2) cyclotron motion with frequency $\omega_c - \omega_m$ about the z-axis, and (3) magnetron motion, a slow drift of the centers of the cyclotron orbits around the z-axis, of frequency ω_m. The frequencies ω_z and ω_c are given by

$$\omega_z = \left(\frac{4eV_o/m}{\rho^2 + 2d^2}\right)^{1/2} \tag{1}$$

$$\omega_c = eB/m \quad , \tag{2}$$

(where e and m are the charge and mass, respectively, of the electron) and ω_m is determined by the relation

$$2\omega_m^2 - 2\omega_m\omega_c + \omega_z^2 = 0 \quad . \tag{3}$$

Loading of the trap with electrons is readily accomplished by means of an electron gun mounted on the back of one end cap. An electron beam can thus be injected through small holes in the end caps, knocking off slow electrons from residual gas atoms inside the trap. After thermal equilibrium is attained, the electrons can be contained for period of hours or more, provided that the residual gas pressure is less than 5×10^{-10} torr. (Previous investigators have reported trapping times of several weeks for residual gas pressures below 5×10^{-11} torr.) Typically, an initial trapped electron number of $< 10^5$ is used.

Thermalization of the electrons in the trap occurs by the mechanism of electron-electron Coulomb collision relaxation, characterized by the Spitzer time constant (Ref. A7)

$$\tau_c = 3.3 \times 10^5 \frac{(kT/e)^{3/2}}{n\ell n\Lambda} \quad ,$$

where n is the electron density in cm^{-3}, Λ is a shielding cutoff parameter, and kT/e is in electron volts (T is the electron temperature). Since

$\ell n\Lambda \sim 15$, typically τ_c is of the order of a few milliseconds under normal conditions of operation. For sufficiently high trapping voltage, the equilibrium electron temperature attained can be fixed by radiative coupling of the z-motion of the electrons to an external tank circuit connected across the end caps. As the electrons oscillate along the axis, they induce image currents in the external circuit (which is usually tuned to resonance at ω_z). Joule heating of the circuit resistance by these currents exponentially damps the electron motion, causing the electron temperature to approach that of the external circuit with relaxation time τ_{zt}. The electron temperature can thus be maintained at any given, known value by injecting white noise (from a temperature-limited diode) into the tank circuit.

Measurement of the number of electrons in the trap at any given time can be accomplished by means of the "bolometric" technique of Dehmelt and Walls (Ref. A2). The noise power of the image currents in the tank circuit, which is proportional to the number of electrons and their temperature, is amplified, heterodyned to an intermediate frequency, filtered and square-law detected (Figure A3). A calibration scale is established by measurements of the noise power at different temperatures and of the tank Q and time constant τ_{zt}. The calibration procedures are detailed in Refs. A2 and A8.

The volume of the trap occupied by electrons can readily be calculated for any given temperature and well depth. This volume is small enough (typically ~ 0.01 cm^3) that it may easily be irradiated by a molecular beam passing through small slits in the ring electrode. The beam used should be designed to provide a uniform density of beam molecules throughout the volume occupied by electrons.

It should be noted that, with positive V_o, negative ions as well as electrons are trapped. Detection and identification of the negative ions can be accomplished by tuning the end cap tank circuit to ω_z as given by Eq. (1), with the appropriate value of q/m, and measuring the noise power generated by the ions. Cyclotron resonance heating can be utilized in order to attain very high mass resolution (Ref. A9). Quantitative measurement of the number of negative ions may be performed with the bolometric technique.

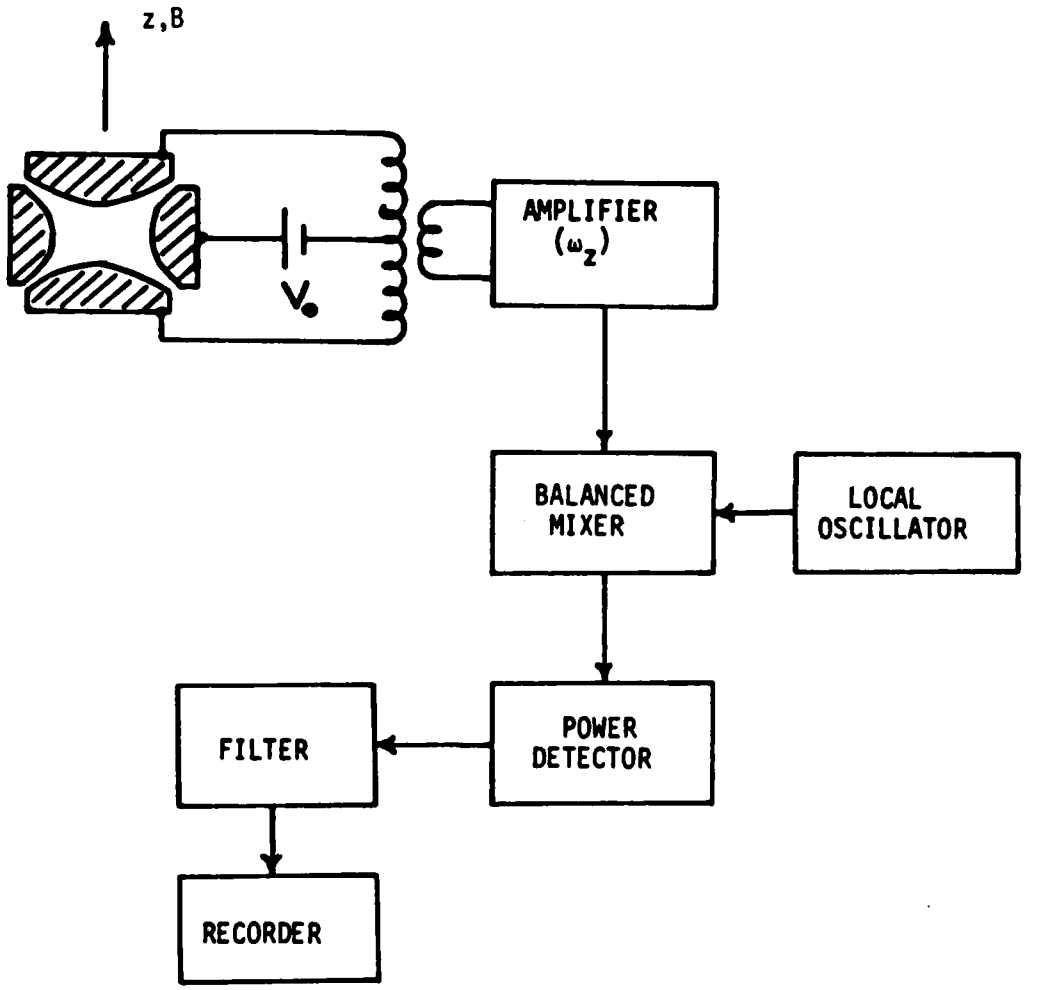

Figure A3. Quadrupole trap detection system

The required value of beam density in the electron trap can be easily estimated. Assuming that the decay time constant for loss of electrons from the trap due to collisions with background gas is large compared with the time over which attachment measurements are to be made, the time dependence of the electron number is given by

$$\ell n\left(\frac{N_o}{N}\right) = \alpha n_b t \quad , \tag{4}$$

where N_o is the initial number of electrons, N is the number remaining after time t, n_b is the H_2WO_4 beam density, and α is the attachment coefficient. The range within which the attachment coefficient for H_2WO_4 is expected to fall is 10^{-8} to 10^{-10} cm^3 sec^{-1}. A convenient time for reaction is $t \sim 1000$ sec, and $\ell n(N_o/N)$ should be ≥ 1 for sufficient accuracy. Eq. (4) then yields a beam density of requirement of $n_b \sim 10^5 - 10^7$ cm^{-3}. (It should be noted that this requirement is not firm, since there is much flexibility in the choice of interaction time, t.) Molecular beam densities in this range are readily obtained for source partial pressures $\leq 10^{-2}$ torr and appropriate dimensions. The minimum attachment rate which can be observed depends upon the rate of loss of electrons from the trap due to momentum transfer collisions with beam molecules. The role of this limitation must be assessed for each circumstance.

The electron trap method does require determination of the molecular beam density for absolute measurements of attachment rates, as in the case of the crossed beam method. A good ultrahigh vacuum system is necessary, and the background vacuum must remain good with the beam source connected and in operation. Construction of the electron trap would probably be more difficult and expensive than that of a trochoidal monochromator electron beam system.

REFERENCES

A1. J. Byrne and P. S. Farago, Proc. Phys. Soc. (London) 86, 801 (1965).

A2. H. G. Dehmelt and F. L. Walls, Phys.Rev. Letters 21, 127 (1968).

A3. D. A. Church and H. G. Dehmelt, J. Appl. Phys. 40, 3421 (1969).

A4. D. A. Church and B. Mokri, Z. Physik 244, 6 (1971).

A5. F. L. Walls and T. S. Stein, Phys. Rev. Letters 31, 975 (1973).

A6. D. Wineland, P. Ekstrom, and H. Dehmelt, Phys. Rev. Letters 31, 1279 (1973).

A7. L. Pitzer, Physics of Fully Ionized Gases (Intersciences, New York, 1962), 2nd ed.

A8. H. G. Dehmelt, in Advances in Atomic and Molecular Physics, edited by D. R. Bates and I. Esterman (Academic, New York, 1967), Vol. 3, p. 53; Vol. 6 (1969), p. 109.

A9. R. A. Heppner, F. L. Walls, W. T. Armstrong, and G. H. Dunn, Phys. Rev. A13, 1000 (1976).

APPENDIX B

INITIAL INVESTIGATION OF ELECTRON ATTACHMENT IN MOLYBDENUM HEXAFLUORIDE AND TUNGSTEN HEXAFLUORIDE

B1. INTRODUCTION

This Appendix summarizes the results of a survey investigation of electron attachment in MoF_6 and WF_6. Although plasma seeding experiments have indicated that these species have high electron attachment rates, very little fundamental research has been done on them. Apparently, there has been only one study of MoF_6 with quasi-monoenergetic electron beams (Ref. B1), and none of WF_6. The present experiment utilizes crossed electron and molecular beams, with electron beam energy resolution far better than that in the prior work on MoF_6. Here only 2-body attachment reactions, such as

$$e^- + MoF_6 \rightarrow MoF_6^- \qquad \text{(direct attachment)}$$

or

$$e^- + MoF_6 \rightarrow MoF_6^+ + F \quad \text{(dissociative attachment)} ,$$

are studied, as contrasted with plasma experiments where other processes (e.g., 3-body attachment, ion-molecule reactions, or charge transfer) may occur.

B2. EXPERIMENT

B2.1 GENERAL

In a beam experiment of this nature, direct measurement of absolute cross sections is difficult, mostly due to the problem of determining the ion collection efficiency. An acceptable alternative is to determine cross sections relative to some known cross section for a similar collision process. Traditionally, SF_6 has to some extent served as a standard for comparison of attachment measurements at very low electron energies, since it has been studied by many investigators. SF_6 exhibits a very large cross section for direct attachment (formation of metastable SF_6^-) at zero electron energy, as well as dissociative attachment leading to SF_5^- with peaks at 0 eV and 0.38 eV. In addition, F^-, F_2^-, SF_4^-, SF_3^-, and SF_2^- are formed with small cross sections

at higher electron energies. Electron attachment in WF_6 and MoF_6 was expected to be similar in many respect to that in SF_6, so it was decided to use SF_6 measurements for determination of cross sections in those gases.

Accordingly, the electron beam system was adjusted for optimum performance with SF_6, especially with regard to the compromise between electron energy spread and ion extraction efficiency. Since the cross section for formation of SF_6^- is essentially a delta-function at zero energy, the SF_6^- ion current as a function of accelerating potential (electron energy) reproduces the electron energy distribution in the beam. The distributions so observed agreed well with those inferred from electron beam retarding curves, yielding some confidence that the apparatus was functioning properly.

B2.2 MoF_6

Since MoF_6 was considered to be less reactive than WF_6, it was studied first. Given the highly toxic nature of the gas, much care was taken to ensure that the gas introduction system for the molecular beam source would remain leak tight. Materials exposed to the MoF_6 were stainless steel, copper, and Teflon. The oven source initially used was made of rolled tungsten foil. Available information indicated that all such surfaces would passivate (acquire stable fluoride coatings) upon exposure to the hexafluorides. It was observed that all internal surfaces become coated with a dark blue substance, presumably an oxide such as Mo_3O_8 (W_3O_8).

In the study of collision processes with reasonably large cross sections, the pressure in the molecular beam source is normally maintained in the range 1-100 μ. The vapor pressure of liquid MoF_6 (b.p. 34°C) is given by (Ref. B2)

$$\log P = 7.766 - \frac{1499.9}{T} ,$$

where P is in torr, and WF_6 (b.p. 17.1°C) is entirely a gas at room temperature. Thus, it was expected that a proper pressure of either gas could be obtained in the source by flowing the gas from a small storage cylinder through a precision leak valve.

Initially, some difficulty was experienced in maintaining a constant pressure of MoF_6 in the beam source. (The source pressure is measured in the

present apparatus with an MKS Baratron differential manometer.) Undoubtedly, some time was required for fluoridation of the source tubing and valves, but much of the instability was traced to molybdenum compound deposits building up on the needle in the leak valve. Gradually this problem was to some extent overcome, and it was usually possible to maintain the pressure reasonably constant for the duration of a set of measurements.

From the results on MoF_6 reported in Ref. B1, it was expected that broad peaks of MoF_6^- and MoF_5^- would appear in the 0 to 3 eV energy range, roughly comparable in magnitude. This was not found to be the case in the present experiments. Sharp peaks of MoF_6^- and, apparently, MoF_5^- were observed at zero energy. A much smaller, broad peak of MoF_5^- was seen in the 0.3-1.5 eV energy range. However, the zero energy peak identified as MoF_5^- did not exhibit a proper dependence on source pressure. In fact, it was nearly independent of indicated pressure above about 3 μ. Furthermore, when the beam source oven temperature was raised, a large increase in MoF_5^- signal was observed, followed by a slow decay back to room temperature signal levels. Such transient effects did not appear upon further raising the source temperature. The tungsten oven source was replaced with a Monel source (since Monel is considered to be inert with respect to MoF_6 and WF_6), but the same behavior was observed.

During these first measurements, the quadrupole mass filter was set for low resolution in order to maximize signal sizes. Mo has seven stable isotopes and the mass numbers to be expected are given in Table 1.

Table 1

MoF_6	MoF_5	$MoOF_4$	% Abundance
206	187	184	15.84
208	189	186	9.04
209	190	187	15.72
210	191	188	16.53
211	192	189	9.46
212	193	190	23.78
214	195	192	9.63

For maximum signal size, it is advantageous to use a mass resolution such that several mass numbers contribute to the signal at any given mass setting of the spectrometer. Using low resolution also minimizes mass discrimination effects when cross section ratios are being determined for different ions. The disadvantage of this procedure is that the mass numbers of the ions being observed are not given accurately by the mass scale reading of the spectrometer.

It was suspected that an impurity might be responsible for much of the observed attachment when Dr. K. Westberg of the Aerospace Corporation pointed out that $MoOF_4$ had been found in all MoF_6 samples used in thermochemical measurements on MoF_6 (Ref. B3). Investigation with high mass resolution and careful mass calibration quickly established that the dominant negative ion produced at zero energy, earlier assumed to be MoF_5^-, was $MoOF_4^-$. The MoF_6^- had been correctly identified.

$MoOF_4$ is a solid at room temperature with a vapor pressure in torr given by (Ref. B4)

$$\text{Log } P = 9.21 - \frac{2854}{T} .$$

The most likely origin of this substance in the present experiment is as an impurity in the MoF_6 sample, although formation through wall reactions in the sample system tubing cannot be yet ruled out. (This particular sample was obtained from RIC, Sun Valley, Calif.) When the source leak valve is opened to the MoF_6 sample, some of the $MoOF_4$ present in the MoF_6 vapor condenses in the beam source and associated tubing. After a period of time, an equilibrium of sorts is apparently established in the source between solid $MoOF_4$ and its vapor such that the partial pressure is a few microns. At that point, it was found possible to pump away the more volatile MoF_6, leaving most of the $MoOF_4$ in the beam source. Then the $MoOF_4^-$ signal was found to be linear with indicated pressure as the $MoOF_4$ pressure gradually decreased, allowing calibration of the cross section relative to SF_6.

B2.3 WF_6

Before the impurity problem in the MoF_6 had been discovered, an attempt was made to observe attachment in WF_6. Source pressure instability problems

were experienced, more severe than with MoF_6. At first, very little attachment was observed (except possibly a small amount of WF_6^- at zero electron energy). After several hours with WF_6 in the source, a small signal identified as WF_5^- appeared at zero electron energy. Again the signal seemed essentially independent of WF_6 pressure, persisting for long periods after the WF_6 has been pumped out of the source. Upon increase of the source oven temperature, the signal rapidly increased by greater than a factor of ten, then slowly decayed back to levels observed before heating.

Because of these difficulties, no attempt was made at quantitative measurements in WF_6 before returning to study of MoF_6. Later, it was realized that the ion observed was probably WOF_4^- from WOF_4 impurity in the WF_6. WOF_4 is a solid at room temperature with a vapor pressure (torr) given by (Ref. B4)

$$\log P = 10.96 - \frac{3605}{T} \quad .$$

Indeed, Hildenbrand (Ref. B5) found WOF_4 impurity in all WF_6 samples used in his thermochemical measurements.

B3. RESULTS AND DISCUSSION

The measured energy dependence of the $MoOF_4$ attachment cross section near zero energy is shown in Figure B1, together with data for SF_6 taken at the same time. The $MoOF_4^-$ curve was normalized in magnitude to that for SF_6^- at the peak, and the electron energy scale was established by considering the SF_6^- peak to be zero energy. (Signals at apparently negative energies are simply a consequence of referencing the energy scale to the peak of the electron energy distribution.) The two curves are identical (within experimental error) and just reproduce the electron beam energy distribution. Thus, the cross section for

$$e^- + MoOF_4 \rightarrow MoOF_4^-$$

is a very sharp peak at zero electron energy (essentially a delta-function).

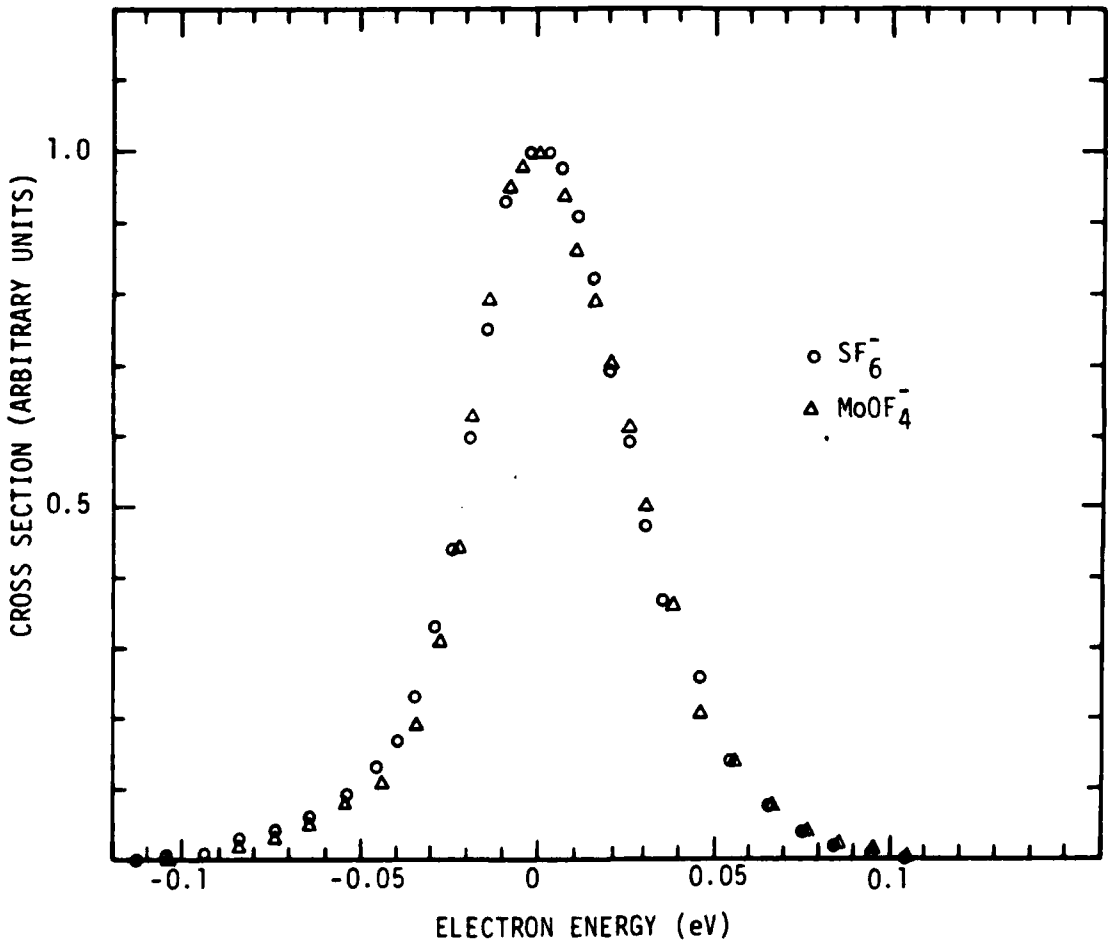

Figure B1. Relative attachment cross sections for SF_6 and $MoOF_4$ vs electron energy at a beam source temperature of 298K. The $MoOF_4^-$ curve is normalized to that for SF_6^- at the peak.

Absolute cross section ratios at room temperature were determined to be

$$\frac{Q[SF_6^-]}{Q[MoOF_4^-]} = 2.4 \quad , \text{ and } \quad \frac{Q[SF_6^-]}{Q[MoF_6^-]} = 110 \quad .$$

Probable error in these ratios is a factor of two. The major source of error is considered to be mass discrimination in the quadrupole filter. Lifetime effects ($MoOF_4^-$ and MoF_6^- formed in this manner are metastable) are probably small, since the electron affinities involved are large. To the extent that mass discrimination is present, the actual cross sections for $MoOF_4^-$ and MoF_6^- would be larger than indicated above (i.e., the ratios given above should be upper limits).

Once the cross section for $e^- + SF_6 \rightarrow SF_6^-$ is specified, the cross sections for attachment to $MoOF_4$ and MoF_6 are determined. Values for the SF_6 cross section found in the literature differ substantially. New measurements of this cross section have been made by Chantry (P. J. Chantry, private communication) and they should be the best to date. The present apparatus yields cross section ratios for SF_6^- to SF_5^- larger than those found by Chantry, but that is to be expected since the energy resolution is a factor of two better than that in Chantry's experiments. Since the observed cross section of a sharp, zero-energy attachment process is a function of the energy-resolution used, the energy-integrated cross section, $\overline{Q}$, which should be independent of resolution, can be used for comparison purposes. Chantry obtained 4.8×10^{-15} cm^2-eV for $e^- + SF_6 \rightarrow SF_6^-$ at room temperature. Using this value,

$$\overline{Q} \geq 2 \times 10^{-15} \text{ cm}^2\text{-eV} \quad \text{for } e^- + MoOF_4 \rightarrow MoOF_4^- \quad ,$$

and

$$\overline{Q} \geq 4.4 \times 10^{-17} \text{ cm}^2\text{-eV} \text{ for } e^- + MoF_6 \rightarrow MoF_6^-$$

in the energy range 0-0.2 eV.

Representative values of the rate for attachment to SF_6 at room temperature are 2.2×10^{-7} cm^3 sec^{-1} (Ref. B6) and 2.7×10^{-7} cm^3 sec^{-1} (Ref. B7). Assuming an average value of 2.5×10^{-7}, we have (at room temperature)

$$R \geq 1 \times 10^{-7} \text{ cm}^3 \text{ sec}^{-1} \quad \text{for } e^- + MoOF_4 \rightarrow MoOF_4^- \quad ,$$

and

$$R \geq 2.3 \times 10^{-9} \text{ cm}^3 \text{ sec}^{-1} \text{ for } e^- + MoF_6 \rightarrow MoF_6^- \quad .$$

From the sketchy observations to date, the signal size for the negative ion observed in WF_6, presumably WOF_4^- formed from WOF_4 impurity, would imply a cross section (and rate) at least as high as that for $MoOF_4^-$.

No temperature dependences have yet been measured for the cross sections reported here. In addition, the identity of the ion observed in the 0.3-1.5 eV energy range in MoF_6 has not yet been established, although it is probably MoF_5^-, nor has the magnitude of the cross section for that peak been determined. It is possible that there is also some MoF_5^- production at zero energy. It is expected that these topics will be further investigated in the present program. Additional work on WF_6 is also planned.

There are several possible reasons for the apparent disagreement between the present results on MoF_6 and those reported by Stockdale, et al. (Ref. B1). Firstly, the energy resolution was a factor of 5-10 better in the present case, and resolution has a profound effect on negative ion cross section shapes, especially where zero-energy processes are involved. Secondly, the MoF_6 filled the electron gun in the previous work, therefore many of the negative ions observed could have been formed on the filament by thermal attachment processes. This cannot happen in a beam experiment, especially with synchronous detection.

The ions MoF_6^-, MoF_5^-, and $MoOF_4^-$ (among others) have been observed at high temperatures in plasma seeding experiments. It is difficult to compare the present results with such experiments, both because of the differences in temperatures and because of possible secondary processes in the plasma (such as charge exchange).

REFERENCES

B1. J. A. D. Stockdale, R. N. Compton, and H. C. Schweinler, J. Chem. Phys. 53, 1502 (1970).

B2. G. H. Cady and G. B. Hargreaves, J. Chem. Soc. (London), 1563 (1961).

B3. D. L. Hildenbrand, J. Chem. Phys. 65, 614 (1976).

B4. G. H. Cady and G. B. Hargreaves, J. Chem. Soc. (London), 1568 (1961).

B5. D. L. Hildenbrand, J. Chem. Phys. 62, 3074 (1975).

B6. F. C. Fehsenfeld, J. Chem. Phys. 53, 2000 (1970).

B7. L. G. Christophorou, D. L. McCorkle, and J. G. Carter, J. Chem. Phys. 54, 253 (1971).